STUDIES ON UNDERWATER PROPAGATION :

DEVELOPMENT OF PROGRAMMABLE ARRAYS

By

P. R. SASEENDRAN PILLAI

THESIS SUBMITTED IN PARTIAL FULFILMENT
OF
THE REQUIREMENTS FOR THE DEGREE
OF
DOCTOR OF PHILOSOPHY

DEPARTMENT OF ELECTRONICS & COMMUNICATION SYSTEMS

UNIVERSITY OF COCHIN

COCHIN 682 022

INDIA

1981

DECLARATION

This is to declare that, the thesis entitled 'Studies On Underwater Propagation: Development of Programmable Arrays' has not previously formed the basis of award for any other degree, diploma, fellowship or any other similar title or recognition.

Cochin - 22,
18 December 1981.

Saseendran Pillai

P.R. SASEENDRAN PILLAI

CERTIFICATE

This is to certify that the thesis entitled 'Studies on Underwater Propagation: Development of Programmable Arrays' which is hereby submitted by Mr. P.R. Saseendran Pillai, to the University of Cochin, in fulfilment of the requirements for the award of the Degree of Doctor of Philosophy, is a record of bona-fide research work carried out by him, under my guidance and supervision, in the Department of Electronics and Communication Systems, University of Cochin, Cochin-22.

C Sridhar

Dr. C.S. SRIDHAR
(Supervising Teacher)
Department of Electronics and Communication Systems,
University of Cochin.

Cochin - 22,
18 December 1981.

ACKNOWLEDGMENTS

The author gratefully expresses his sincere gratitude tc Dr. C.S. Sridhar, Reader, Department of Electronics and Communication Systems, University of Cochin, for his able guidance, sincere interest, valuable advices and inspiring encouragements for the successful completion of this work.

The author is extremely grateful to Dr.K.G. Nair, Professor and Head of the Department of Electronics and Communication Systems, University of Cochin, for his interest in the topic and for making necessary arrangements for carrying out this work at the Department laboratory and an R and D laboratory.

The author gratefully thanks his colleague, Smt. T. Rajalakshmy, with whom he made numerous stimulating discussions and all her suggestions and comments for the improvement of this work are gratefully acknowledged.

The author is thankful to Mr. Poulose Jacob for his dedicated help, to Dr.(Mrs.) P V Deo, Lecturer, Department of Electronics and Communication Systems, Mr. A. Vijayakumar, Department of Mathematics and Statistics and to Mr. Raveendran, Electronics Section, C W I S L,

University of Cochin, for his co-operation in running the computer programs. The author also expresses his sincere thanks to the other staff of the Department of Electronics and Communication Systems.

The author is grateful to the Department of Atomic Energy, Government of India, for the fellowships and contingency grants awarded to him. He gratefully acknowledges the authorities of University of Cochin for awarding the Cochin University Junior Research Fellowship at the initial stages of his work and for providing necessary facilities to carry out this work.

The author would like to express his sincere thanks to the authorities of Naval Physical and Oceanographic Laboratory, Cochin for all their helps especially for providing the library facilities and for supplying some of their transducers under 'Trial and Return' condition.

Sincere help and co-operation from Mr. C.S. Sivakumar, Mr. K.M. Mathew, Mr. C.B. Muraleedharan, Mr. V.M. Asharaf, Mr. V.M. Peter and Mr. N. Appukuttan Nair, for making this thesis in its present form are gratefully acknowledged.

C O N T E N T S

LIST OF SYMBOLS USED

Symbol		Description
dB	:	decibel
V	:	volt
μb	:	microbar
Hz	:	hertz
kHz	:	kilohertz
LPA	:	loosely packed array
CPPA	:	closely packed planar array
SAAT	:	shading by an average amplitude in time
HPBW	:	half power beam width
I_r	:	the ratio of the acoustic intensity to the reference acoustic intensity
I	:	intensity of sound wave
I_o	:	the reference acoustic intensity
p_r	:	the ratio of acoustic pressure to the reference acoustic pressure
p	:	acoustic pressure
p_o	:	the reference acoustic pressure
dyn	:	dyne
μPa	:	micropascal
m	:	metre
cm	:	centimetre
mm	:	millimetre
W	:	watt

N	:	newton
λ	:	the wavelength of acoustic radiation at the design frequency, in water
V_o	:	the voltage generated in the reference elements, of the loosely packed array, due to the incident acoustic radiation.
R	:	the voltage response of transducer elements used in the array
ω	:	angular frequency of acoustic radiation
θ	:	the angle which the incident acoustic radiation makes with the line passing through the centre of the array and normal to its plane
$\sum$	:	the notation for summation
n	:	an integer
U	:	the minimum phase term with respect to the reference elements of the LPA
d	:	the minimum spacing between the elements in the LPA
V_1	:	the voltage generated in all the elements of cross C_1
j	:	the complex quantity $\sqrt{-1}$
e	:	the base of natural logarithm
φ	:	angle between the two crosses C_1 and C_2
V_2	:	the voltage generated in all the elements of cross C_2
V'	:	the total array voltage
N'	:	the total number of elements in the LPA format
b(θ)	:	beam pattern of the 43-element array format
b'(θ)	:	beam pattern of the 63-element array format

$b_1(\theta)$	:	beam pattern of the 45-element array format
$b_2(\theta)$	:	beam pattern of the 65-element array format
λ'	:	wavelength of acoustic radiation in air
s	:	second
ms	:	millisecond
μs	:	microsecond
f_1, f_2	:	primary frequencies used for the generation of the difference frequency signal
θ'	:	the angle which an observer makes with the axis of the array
$D(\theta')$	:	the two dimensional directivity pattern of the difference frequency signal
S	:	the aperture area of the LPA format
A_f	:	the aperture factor
α_1	:	absorption coefficient of one of the primary frequencies, f_1
α_2	:	absorption coefficient of the other primary frequency, f_2
α'	:	absorption coefficient of the difference frequency signal
A'	:	the absorption function, of value $\alpha_1 + \alpha_2 - \alpha' \cos \theta'$
λ''	:	wavelength of the acoustic radiation at the difference frequency
K'	:	wavenumber at the difference frequency
a	:	radius of the radiating aperture of the LPA format
$J_1(x)$	:	the first-order Bessel function of argument x
nep	:	neper

Q	:	quality factor
Q_e	:	electrical Q
Q_m	:	mechanical Q
s'	:	elastic constant of the material of the transducer, measured in m^2/N
l	:	thickness of the active material
A	:	area of the radiating face of a transducer element
M	:	equivalent mass of the transducer when radiating into infinite medium
M_1, M_2	:	the values of M under the two specific cases of the reflected signal opposing and enforcing the vibration
R_m	:	mechanical resistance of the transducer when radiating into infinite medium
R_{m1}, R_{m2}	:	the values of R_m under the two specific cases of the reflected signal
C_m	:	compliance of the transducer when radiating into infinite medium
C_{m1}, C_{m2}	:	the values of C_m under the two specific cases of the reflected signal
f_r	:	resonance frequency of the transducer
ω_r	:	angular resonance frequency of the transducer
η	:	the efficiency of the transducer when radiating into infinite medium
η_1, η_2	:	the values of η under the two specific cases of the reflected signal
D_a	:	diameter of the admittance diagram of the transducer with air-loading
D_c	:	diameter of the admittance diagram of the transducer with castor oil-loading

G_{ma}	:	maximum conductance of the transducer with air-loading
G_{mc}	:	maximum conductance of the transducer with castor oil-loading
ρ	:	density of the fluid medium into which the transducer is radiating
c	:	velocity of propagation of acoustic radiation in water
C_o	:	static capacitance of the transducer
C	:	coulomb
α	:	transformation ratio of the element
e'	:	piezo-electric stress coefficient
R	:	electrical equivalent resistance of the transducer
k_c	:	electromechanical coupling coefficient
u	:	velocity amplitude of the transducer when radiating into the infinite medium
u_1, u_2	:	the values of u under the two specific cases of the reflected signal
F(t)	:	time-varying external driving force
F	:	amplitude of the time-varying force F(t)
kg	:	kilogram
F'(t)	:	time-varying reflected signal
k'	:	a quantity depending on the transducer position and the material of the container
β	:	the phase lag between the driving signal and the signal across the transducer, when radiating into the infinite medium
β'	:	the phase term in the reflected signal, due to the travel time

h	:	height of the castor oil column below the radiating face of the transducer
β_1, β_2	:	the values of β under the two specific cases of the reflected signal
θ_1, θ_2	:	the phase term of the effective driving signal under the two specific cases of the reflected signal
a'	:	a quantity defined by $\sqrt{(1 + k'^2 - 2k' \cos \beta_1)}$
b'	:	a quantity defined by $\sqrt{(1 + k'^2 + 2k' \cos \beta_2)}$
v	:	voltage across the transducer element
P	:	average acoustic power radiated into the infinite medium
P_1, P_2	:	the values of P under the two specific cases of the reflected signal
P_e	:	electrical power pumped to the transducer
p_1, p_2	:	the values of p under the two specific cases of the reflected signal
i	:	current in the circuit when the transducer radiates into the infinite medium
i_1, i_2	:	the values of i under the two specific cases of the reflected signal

LIST OF FIGURES

LIST OF TABLES

STUDIES ON UNDERWATER PROPAGATION:

DEVELOPMENT OF PROGRAMMABLE ARRAYS

CHAPTER I

I N T R O D U C T I O N

1.1 Importance of Acoustic Radiation for Underwater Propagation

The study of 'Underwater Sound' is important, as it is the most powerful aid in obtaining informations in the sea. Acoustic radiation propagates much larger distances, in the ocean, the detectable range being several thousand kilometres. The propagation of electromagnetic waves through water is limited to the very high wavelength zone, of the order of several kilometres, where the resolution and directional beam formation are quite impossible[1a]. While, in air, the attenuation of light in the visible region is lesser than that of sound, the reverse is the case in oceans.

1.2 Historical Survey

The field of 'Underwater Acoustics', though it originated too deep in the past [2], until recently had its applications limited to naval operations. Historically, the first experiment [3a] in this branch was carried out by Daniel Colladon, a Swiss physicist and

Charles Sturm, a French mathematician, by measuring the velocity of sound in the Lake Geneva, in 1827, to a surprising degree of accuracy, by noting the time interval between the striking of a bell and a light flash. The first device, developed in the field of 'Underwater Sound' was the submarine bell used in offshore navigation. During the time of the first world war, an underwater echo-ranging or echo-location was developed and used for military purposes under the name 'ASDIC' [1a]. From the time of second world war onwards, ASDICs are being used both in military and non-military fields. Since ASDIC has a certain degree of naval implications, it is now-a-days referred to as SONAR. Important military and nonmilitary applications of 'Underwater Sound' [1a],[3a] are listed in appendix I, under tables A.I.1 and A.I.2, respectively.

Research in the field of 'Underwater Sound' is reported to have achieved considerable progress during the period of second world war. Some of the observations made in this field by a large group of scientists organised by the National Defence Research Committee, which were once classified, are now reported as the NDRC Division 6 Summary Technical Reports.

Though the field of 'Underwater Acoustics' had only naval implications at the beginning and its origin

can be traced back to the world war periods, its use at present extends to nonmilitary fields such as in the collection of maximum resources out of the sea.

1.3 A Brief Description of the Present Work

The work herein presented includes the designing of underwater transducer arrays, taking into account the 'interaction effects' [3c] among the closely packed radiators.

Methods of minimizing the 'interaction effects' by modifying the radiating aperture, are investigated. The need for this study arises as it is one of the important peculiar limitations that stands in the way of achieving maximum range of transmission of acoustic signals.

Application of the modified array format for the generation of narrow beam low frequency sound waves, through nonlinear interactions, is discussed.

Other techniques that can be advantageously exploited in array synthesis are also investigated.

1.4 Past Work in the Field

A large number of designs of underwater transducer elements and arrays [4b],[5] - linear, plane circular and of various other shapes - are reported in open

literature. In most of those arrays, shading was employed, through suitable control measures over the beam pattern of the particular array configuration. In amplitude shading, the response of various elements or various sets of elements in the array are modified so as to get the most suitable beam pattern, as per the need. Different shading mechanisms are employed, of which the important mechanisms involve 'Binomial Shading' giving rise to a main lobe with the total absence of side lobes [3b] and 'Dolph-Chebyshev Shading' [6],[7], yielding the narrowest main lobe for a specified side lobe level. Control can be exercised on the array for adjusting the beam pattern at the cost of array sensitivity. It is to be borne in mind that heavy shading cannot be adopted under conditions of low signal-to-noise ratio [3b].

In the array design presented in [4b], a considerable amount of shading is introduced. The circular array format reported here is composed of 19 identical PZT transducer elements arranged very close to each other, the analysis treated it as a continuous distribution, ignoring the interaction effects among the closely packed radiators. In this array format, the sensitivities of the elements followed the shading formula 0.4, 0.8, 1, 0.8 and 0.4 and the half power beam width (HPBW) is 11^{o} with a side lobe suppression of 20 dB with reference

to the main beam, having an array sensitivity of -92 dB re 1V/μb.

In the array design reported in [5], details of shading mechanisms are not mentioned. The paper presents the design of high efficiency transducer elements and details of their arrangements on the mounting. Beam patterns of 22, 84 and 432 - element array configurations and their side lobe levels are also presented. Though, a detailed design is reported, nothing is mentioned regarding the shading.

Narrow beam transducers with suppressed side lobes are manufactured by Edo Western Corporation [9],[10], one of the leading manufacturers of underwater transducers. In one of their catalogues, they claimed to have produced a 24 kHz transducer with 11^{o} HPBW and side lobes suppressed below 25 dB, with reference to the main lobe through shading techniques.

A number of other papers on array design [4c], interaction effects [11]-[19] and nonlinearity [20]-[35] are reported in literature.

1.5 Scheme of the Present Work

The high power limitations of transducers used in sonar projector arrays are,

1. The 'interaction effects' among the closely packed elements
2. The on-set of 'cavitation'
3. Dynamic strength of the active material
4. Fall in efficiency due to internal mechanical loss
5. Depolarization of the ceramic due to
   (i) temperature rise and
   (ii) high electric field
6. Increase in electrical loss at high electric field and
7. Magnetic saturation in magnetostrictive types.

Of these limitations, the prominent are (1) and (2). The first one is considered in this work and the possible solution to this problem, which can be easily realised is presented.

Though different array designs and shading methods are reported among the past works, the papers quoted in 1.3 are examples for the arrays with closely packed elements. It is felt that the closely packed elements will introduce the problem of acoustic interactions among the radiators themselves, due to which the effective measured acoustic output will be reduced from the expected value. An array format with loosely packed elements, to reduce the 'interaction effects', is presented in Chapter II.

The loosely packed array (LPA) format presented in chapter II has the unique advantage that closely packed planar arrays (CPPA), the elements of which are arranged half-a-wavelength apart can be converted to the proposed format by selectively switching only those elements that produce the required beam pattern. The selective switching of the elements of a CPPA is achieved by a microprocessor based switching system. The design details of this system is described in chapter III. The flow-chart and the program for switching the selected elements of a CPPA is given in appendix III.

The drawbacks of the LPA format can be rectified through a CPPA, working in conjunction with the switching system. The switching system and the CPPA can be suitably implemented to achieve the lobe switching, shading by an average amplitude in time (SAAT) and higher array gain, with suitable programs. The development of a programable array using a CPPA and the switching system is described in chapter IV.

The LPA format presented in chapter II, conforming to Carson's [11] suggestion is capable of producing narrow beam low frequency sound waves. Application of this array format for the generation of low frequency sound waves through nonlinear interactions is discussed in chapter V.

Experimental investigations on the effects of finite medium on the performance characteristics of ceramic transducer elements revealed the variations in resonance frequency, impedance at resonance, the Q-factor, the efficiency of radiation and the related parameters, due to change in loading caused by the standing wave field. Variations of conductance and susceptance of magnetostrictive transducer elements in a standing wave field, with depth of immersion, at a frequency which corresponds to the resonance frequency in free-field or constant-field conditions are reported in [36]. A slightly different variation of impedance at resonance, from those reported, is observed for an electrostrictive transducer and this variation is presented in chapter VI, taking into account the observed resonance frequency variation with depth of immersion of the radiating face of the transducer. Applications of this effect towards array synthesis and non-linearity study are also presented.

Finally, the highlights and a brief survey of the results presented in this work towards the scope for future developments is discussed in chapter VII.

1.6 The New Reference Unit

In underwater propagation studies, since the intensity and pressure magnitudes vary over a wide range,

the unit called decibel (dB) had been developed, which can handle large quantities without the necessity of large exponents. This unit is defined as,

$$\text{Sound level in dB} = 10 \log I_r$$

$$= 20 \log p_r$$

where

$$I_r = \frac{I}{I_o},$$

I being the acoustic intensity and I_o the reference acoustic intensity

and

$$p_r = \frac{p}{p_o},$$

p being the acoustic pressure and p_o the reference acoustic pressure.

Reference acoustical quantities customarily used were 1 dyn/cm^2 (μb) and 0.000204 dyn/cm^2. As per the recommendations of the American National Standards Institute [37], the new reference unit of acoustical intensity is the intensity of a plane wave having an rms pressure of

1μPa or 10^{-5} dyn/cm². This intensity corresponds to 0.64×10^{-22} s·W/cm². The various relations are,

$$1 \text{ Pa} = 1 \text{N/m}^2$$

$$1\mu\text{b} = 1 \text{ dyn/cm}^2$$

$$1 \text{ Pa} = 10 \ \mu\text{b}$$

CHAPTER II

DESIGN CONSIDERATIONS FOR A LOOSELY PACKED ARRAY

2.1 Introduction

A radiator will have a certain form of energy distribution with respect to its orientation. For a single element system - a non-Langevin type - the energy distribution will be almost omnidirectional. A number of elements used in various locations will have certain directional characteristics, that render its usefulness in carrying out safe communications.

Though a single transducer element serves the purpose in research and measurements, it cannot be used in secure communications, from one submarine to another or from war-ships to submarines in the vicinity of an under-sea enemy camp or in other applications involving the direction finding of an object, detection of sound source etc.. Direction finding of an underwater object and undersea explorations will convey false informations unless the transducer system used in the underwater sensor is a directional one. Also, due to noise and reverberation pick-ups, a non-directional transducer will introduce

ambiguity in detection whenever it is used as a hydrophone and will insonify most of the space around it whenever used as a projector. It is evident from the articles found in open literature that the narrower the beam, the higher will be the side lobe level. Again, the higher the side lobe level, the more will be the ambiguity in detection.

A directional transducer system may comprise either a single transducer, whose radiating face is so designed as to get the desired directivity pattern, at the cost of transducer sensitivity, or an array of non-directional transducer elements whose arrangements, spacings and the mode of excitation provide the required beam pattern, or a combination of these two. The advantages of using an array of elements in a transducer system, other than the directionality are enhanced sensitivity and improvement in signal-to-noise ratio.

Significant features of the transducers used in modern sonar systems are,

1. Improved directivity
2. Large aperture with high power capability
3. High efficiency
4. Capability to radiate at low frequencies
5. Large bandwidths for passive listening sonars

Keeping in mind the first two features, a loosely packed array (LPA) is designed [42], with limited number of elements. In this array design, elements are spaced, taking into account both 'interaction effects' among the radiators and the interaction of the radiations, so as to produce narrow beams with side lobes suppressed below a favourable level, in some directions.

2.2 Shading Methods

In linear and planar arrays, narrow beams are achieved by either sacrificing the transducer sensitivity or the side lobe level. The first side lobe level will occur at 13.2 dB below the main beam and minor lobes will be at 17.8 dB, 20.8 dB, 23 dB, 24.7 dB etc., below the main one [4b]. Various shading methods are employed to control these side lobe levels and beam width. Binomial shading [3b], [4b] will produce a wide beam with reduced side lobe level, while edge-distribution produces a narrow beam with side lobes of the same amplitude as the main beam. Though, at the first observation, it seems that a combination of these two techniques can produce a narrow beam with suppressed side lobes, further investigations proved it to be a discouraging combination. However, Dolph [8] has suggested an amplitude distribution, based on the properties of the Chebyshev polynomials, known as

Dolph-Chebyshev distribution. Here again, there is an optimization that, for a desired side lobe level, the beam width will be minimised or for a desired beam width the side lobe level will be less. One of the main disadvantage of shading is the reduction in the array sensitivity.

2.3 Theoretical Analysis of LPA Format

In almost all the array designs, reported in open literature, identical elements are closely packed at distances slightly less than half-a-wavelength - approximately 0.48λ , where λ is the wavelength of acoustic radiation, at the design frequency. The significant drawback imposed by the close packing is the 'interaction effects' [3c],[11] among the radiating elements of a projector array. Due to this effect, the acoustic radiation emitted by each element of the array will be absorbed by the neighbouring ones, thereby reducing the acoustic output and deteriorating the beam pattern. This interaction effect should be minimised in arrays that are intended to radiate large acoustic power and to produce undistorted narrow beams. Although, various control measures are available to reduce the interaction effects, the most simple among them is by increasing the spacing of most of the elements, as suggested by Carson [11] and thus

minimising the mutual radiation impedance [12],[13], which is the root cause of interaction effect. Based on these requirements, a loosely packed array is designed with 43 elements whose radiating aperture is almost circular and in which the elements are arranged along two crosses, which are inclined at an angle to get the most favourable beam pattern.

The array configuration shown in Fig.2.1 has two crosses C_1 and C_2, C_1 being composed of two mutually perpendicular line arrays A and C, while the mutually perpendicular line arrays B and D constitute the cross C_2. The spacings between the elements in C_1 and C_2 are $\lambda/2$ and λ, respectively.

Consider a beam of plane sinusoidal sound wave of unit pressure incident on the transducer face at an angle θ, to the line passing through the centre of the array and normal to its plane, so that the voltages generated in each element in the line array A are in the same phase. Let this voltage be [3b],

$$V_o = R \cos \omega t \qquad (2.1)$$

where

R = voltage response, assumed to be the same for all the elements of the array and

ω = angular frequency of the acoustic radiation.

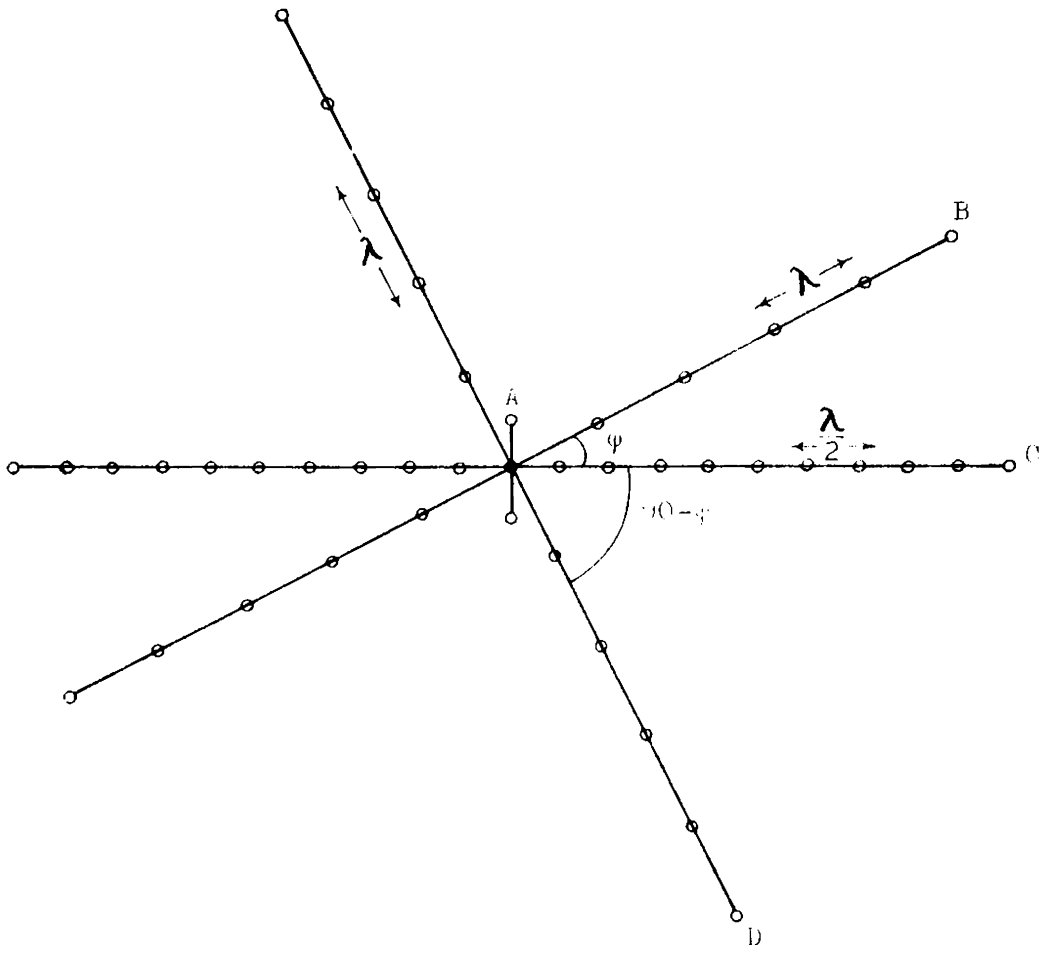

Fig. 1.1 : Front view of the LPA format

The voltages generated in elements to one side of those producing the reference voltage, given by (2.1), will lag in phase, while to the other will lead. The total voltage generated in C_1 will be,

$$V_1 = 3R \cos \omega t + R \sum_{n=1}^{10} [\cos (\omega t - nU) + \cos(\omega t + nU)]$$

where the phase term U is given by

$$U = \frac{2\pi}{\lambda} d \sin \theta$$

$$= \pi \sin \theta,$$

d being the spacing between elements in C_1.

In complex notation, this voltage takes the form,

$$V_1 = R [3 + \sum_{n=1}^{10} (e^{jnU} + e^{-jnU})] e^{j\omega t}$$

$$= R [3 + 2 \sum_{n=1}^{10} \cos (nU)] e^{j\omega t}$$

Neglecting the time dependence and considering array elements of unit response,

$$V_1 = 3 + 2 \sum_{n=1}^{10} \cos (nU)$$

The phase delays for different elements in the line array B are $\pm$ 2U cos φ, $\pm$ 4U cos φ, $\pm$ 6U cosφ, $\pm$ 8U cos φ

and $\pm$ 10U cos φ, while those in D are $\pm$ 2U sin φ, $\pm$ 4U sin φ, $\pm$ 6U sin φ, $\pm$ 8U sin φ and $\pm$ 10U sin φ, where φ is the angle between the line arrays B and C.

Considering unit response elements and neglecting the time dependence, as above, the voltage generated in C_2 takes the form,

$$V_2 = 2\left[\sum_{n=1}^{5} \cos (2nU \cos \varphi) + \sum_{n=1}^{5} \cos (2nU \sin \varphi)\right]$$

The total array voltage is

$$V' = V_1 + V_2$$

$$= 3 + 2 \left[\sum_{n=1}^{10} \cos (nU) + \sum_{n=1}^{5} \cos (2nU \cos \varphi) + \sum_{n=1}^{5} \cos (2nU \sin \varphi)\right]$$

The beam pattern for this array is

$$b(\theta) = \left(\frac{V'}{N'}\right)^2$$

$$= \frac{1}{1849} \left\{ 3 + 2 \left[\sum_{n=1}^{10} \cos (nU) + \sum_{n=1}^{5} \cos(2nU \cos \varphi) + \sum_{n=1}^{5} \cos (2nU \sin \varphi)\right] \right\}^2 \qquad (2.2)$$

where N' = 43, the total number of elements in the array.

Similar analysis for an array configuration with 20 elements additionally placed in C_2, arranging 5 elements along each of the extreme ends of the line arrays B and D, at the respective spacing, leads to the beam pattern,

$$b'(\theta) = \frac{1}{3969} \left\{ 3 + 2 \sum_{n=1}^{10} [\cos (nU) + \cos(2nU \cos \varphi) + \cos (2nU \sin \varphi)] \right\}^2 \qquad (2.3)$$

It is to be pointed out that the beam patterns of these 43 and 63-element array formats lack symmetry. This departure from symmetry of the beam patterns can be rectified, to some extent, by adding elements to the line array **A**, symmetrically on both of its sides at $\lambda/2$ spacing. The beam pattern corresponding to the 45 and 65-element arrays can be shown to be,

$$b_1(\theta) = \frac{1}{2025} \left\{ 5 + 2 \left[\sum_{n=1}^{10} \cos (nU) + \sum_{n=1}^{5} \cos(2nU \cos \varphi) + \sum_{n=1}^{5} \cos (2nU \sin \varphi) \right] \right\}^2 \qquad (2.4)$$

and

$$b_2(\theta) = \frac{1}{4225} \left\{ 5 + 2 \sum_{n=1}^{10} [\cos (nU) + \cos (2nU \cos \varphi) + \cos (2nU \sin \varphi)] \right\}^2 \qquad (2.5)$$

In an analogous manner, beam patterns for the 47, 67, 49, 69, etc. element arrays can be derived.

It is to be noted that the dimensions of the radiating aperture of the 63, 65, 67 ... arrays differ from those of 43, 45, 47 ... element ones.

2.4 Theoretical Results

Beam patterns for the 43 and 63-element array configurations given by (2.2) and (2.3) are shown in Fig.2.2(i) and Fig.2.2(ii), respectively. Beam patterns are evaluated for other spacing and various orientations, φ. The variation of the most intense side lobe level and the intensity at 90° to the axis of the array for the 43 and 63-element arrays for different orientations are shown in table 2.1.

Also, the spacings between the elements in C_1 and C_2 are slightly changed. The spacings between the elements in C_1 are varied in the range 0.4λ to 0.6λ and those in C_2 in the range 0.8λ to 1.2λ. The results of these evaluations are briefly represented in tables

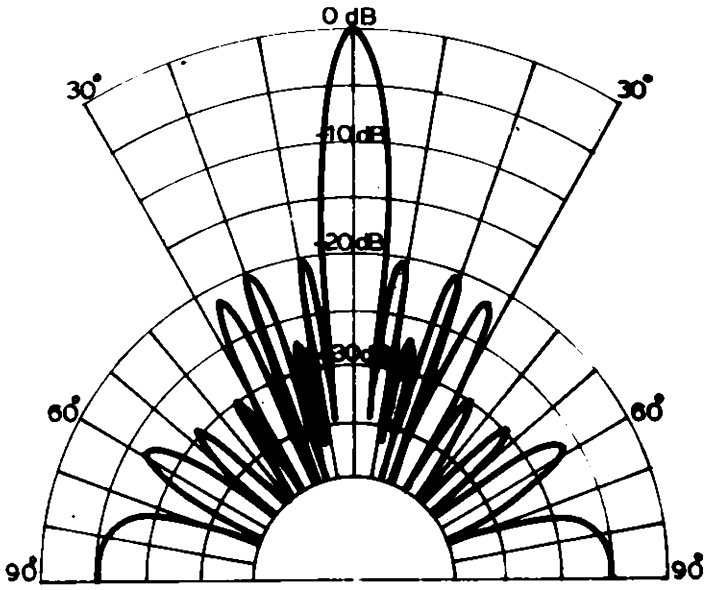

Fig. 2.2(i)

Beam pattern for the 43-element LPA format

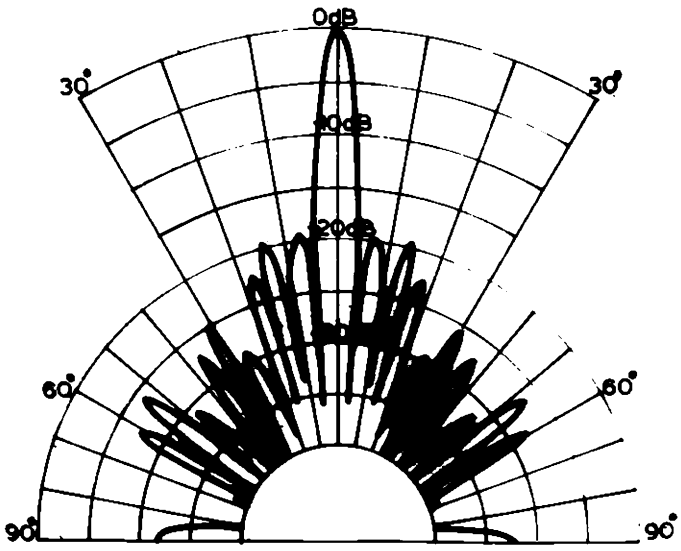

Fig. 2.2(ii)

Beam pattern for the 63-element LPA format

Table 2.1

Variation of the most intense side lobe level and the intensity at $\theta = 90^{\circ}$ for the 63 and 43-element array formats, for different orientations between C_1 and C_2

Angle between the crosses φ (in degree)	63-element array		43-element array	
	Most intense side lobe level (in dB)	Intensity at 90° with respect to the reference elements (in dB)	Most intense side lobe level (in dB)	Intensity at 90° with respect to the reference elements (in dB)
15	-19.15	-19.15	-12.42	-12.42
16	-20.00	-22.46	-13.69	-13.69
18	-20.03	-31.68	-16.32	-16.64
20	-18.23	-24.95	-18.13	-18.94
22	-17.52	-24.31	-17.83	-20.66
24	-17.60	-80.70	-18.01	-24.32
26	-18.36	-31.83	-18.73	-40.07
28	-18.70	-25.54	-19.76	-28.16
30	-19.20	-25.47	-19.83	-24.42
32	-19.19	-40.10	-18.52	-29.85
34	-18.54	-31.84	-17.51	-35.18
36	-17.46	-30.07	-16.72	-24.42
38	-16.68	-26.92	-16.13	-22.84
40	-16.14	-46.66	-15.70	-25.79
42	-15.81	-54.34	-16.33	-36.12
44	-15.64	-31.12	-16.17	-39.53
45	-15.62	-29.35	-15.28	-36.91

Table 2.2

Variation of the intense side lobe level and the intensity at $\theta = 90^{\circ}$, for the 43-element array format, for slight changes in the spacing between the elements.

43-element array

Spacing between elements in cross C_1 (in λ)	Spacing between elements in cross C_2 (in λ)	Diameter of the array (in λ)	Theoretically evaluated HPBW (in degrees)	Most intense side lobe level (in dB)	Intensity level at 90° with respect to the reference elements (in dB)
0.4	0.80	8.0	7	-20.53	-34.78
0.42	0.84	8.4	7	-20.45	-26.92
0.44	0.88	8.8	6.5	-20.43	-28.32
0.46	0.92	9.2	6	-20.43	-46.92
0.48	0.96	9.6	6	-20.45	-29.04
0.50	1.00	10.0	6	-20.53	-25.49
0.52	1.04	10.4	6	-20.61	-36.06
0.54	1.08	10.8	5	-20.44	-20.93
0.56	1.12	11.2	5	-13.26	-13.27
0.58	1.16	11.6	5	-11.333	-11.334
0.60	1.20	12.0	5	-11.32	-14.22

Table 2.3

Variation of the intense side lobe level and the intensity at $\theta = 90^{\circ}$ for the 63-element array format corresponding to slight changes in the spacing between the elements.

63-element array

Spacing between elements in cross C1 (in λ)	Spacing between elements in cross C2 (in λ)	Diameter of the array (in λ)	Theoretically evaluated HPBW (in degrees)	Most intense side lobe level (in dB)	Intensity level at 90° with respect to the reference elements (in dB)
0.4	0.8	16	5	-19.63	-26.26
0.42	0.84	16.8	5	-19.73	-50.09
0.44	0.88	17.6	5	-19.61	-28.40
0.46	0.92	18.4	4.5	-19.55	-41.108
0.48	0.96	19.2	4	-19.75	-47.11
0.50	1.0	20.0	4	-19.59	-32.17
0.52	1.04	20.8	4	-19.65	-30.683
0.54	1.08	21.6	3.75	-19.63	-20.44
0.56	1.12	22.4	3.5	-19.75	-25.05
0.58	1.16	23.2	3.5	-9.09	-9.09
0.60	1.20	24	3	-8.88	-14.65

2.2 and 2.3, respectively, for the 43 and 63-element arrays.

The beam patterns for the 45 and 65-element array formats given by (2.4) and (2.5) are shown in Fig.2.3(i) and 2.3(ii), respectively. The results of the evaluations of the beam patterns of 45, 65, 47, 67, 49 and 69-element arrays for various values of φ are given in table 2.4, 2.5 and 2.6, respectively. Also, these results show slight variations, if the spacings between the elements are changed from 0.4λ to 0.6λ in cross C_1 and 0.8λ to 1.2λ in cross C_2. From these evaluations, the actual spacings between the elements in C_1 and those in C_2 can be accurately determined.

From the tables 2.1, 2.4, 2.5 and 2.6, the angles of orientation φ, for the most favourable beam patterns, corresponding to different array formats are obtained. It is to be noted from the beam patterns that the beam widths are of the same order as in the nomograms for closely packed plane circular arrays, found elsewhere in literature[3a],[38]. The table 2.7 compares the beam widths predicted by these nomograms with the calculated one, at a frequency of 20 kHz.

The effect due to the back radiation can be minimised by either packing, the rear side of each element,

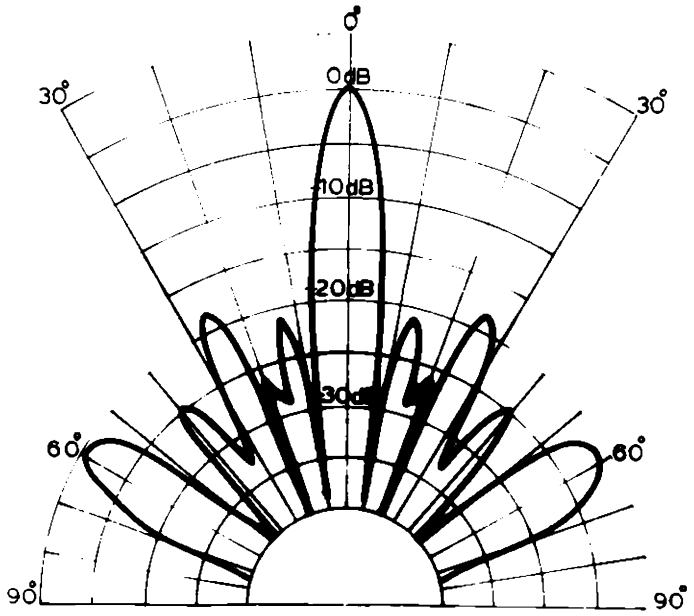

Fig. 2.3(i)

Beam pattern for the 45-element LPA format

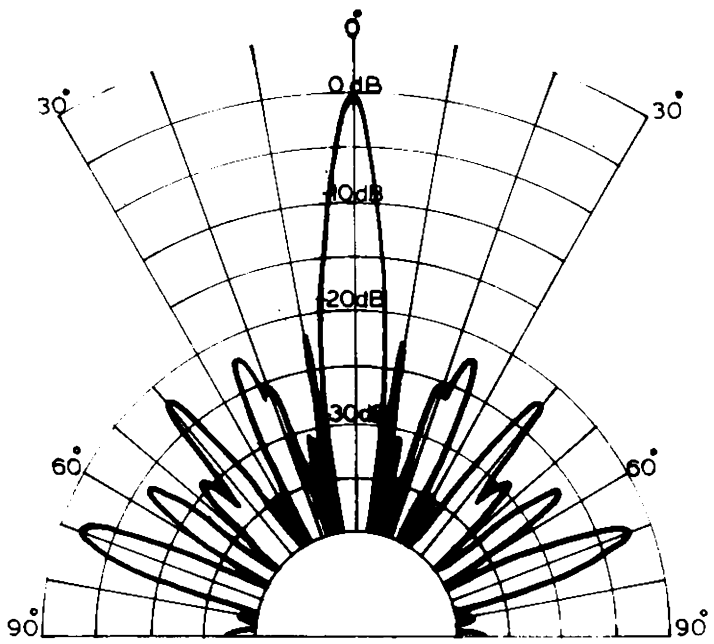

Fig. 2.3(ii)

Beam pattern for the 85-element LPA format

Table 2.4

Intense side lobe levels and the intensity at 90°, for the 65 and 45-element array formats for different values of φ

Angle between the crosses φ (in degrees)	65-element array		45-element array	
	Most intense side lobe level (in dB)	Intensity at 90° with respect to the Reference elements (in dB)	Most intense side lobe level (in dB)	Intensity at 90° with respect to the reference elements (in dB)
15	-17.22	-17.22	-11.27	-11.27
16	-19.67	-19.67	-12.32	-12.32
18	-20.66	-25.03	-14.40	-14.65
20	-21.11	-32.39	-15.75	-16.34
22	-20.16	-31.00	-17.15	-17.52
24	-20.27	-30.26	-18.48	-19.78
26	-17.95	-25.10	-19.03	-25.36
28	-17.21	-21.72	-18.27	-42.97
30	-17.26	-21.68	-18.14	-40.21
32	-18.03	-33.47	-18.62	-37.24
34	-19.50	-44.47	-19.70	-24.28
36	-21.67	-24.27	-19.16	-19.83
38	-22.21	-22.56	-18.53	-18.91
40	-22.90	-29.05	-20.36	-20.58
42	-17.97	-30.77	-19.88	-24.52
44	-17.77	-24.77	-19.52	-29.27
45	-17.75	-23.90	-18.41	-30.22

Table 2.5

Variation of the intense side lobe and the intensity at $\theta = 90^{\circ}$ for the 67 and 47-element array formats for different values of φ

Angle between the crosses φ (in degrees)	67-element array		47-element array	
	Most intense side lobe level (in dB)	Intensity at 90° with respect to the reference elements (in dB)	Most intense side lobe level (in dB)	Intensity at 90° with respect to the reference elements (in dB)
15	-15.73	-15.73	-10.34	-10.34
16	-17.68	-17.68	-11.24	-11.24
18	-18.44	-21.49	-12.96	-13.15
20	-19.31	-43.65	-14.04	-14.50
22	-19.70	-52.00	-15.11	-15.39
24	-17.66	-24.49	-16.10	-17.03
26	-16.32	-21.53	-16.50	-20.52
28	-15.72	-19.22	-15.95	-26.13
30	-15.77	-19.19	-15.86	-27.57
32	-16.39	-25.95	-16.21	-25.08
34	-17.54	-28.95	-16.97	-19.03
36	-19.18	-20.99	-17.03	-17.07
38	-19.57	-19.82	-16.14	-16.41
40	-20.11	-23.86	-17.53	-17.58
42	-20.05	-24.74	-17.68	-20.05
44	-18.72	-21.32	-17.04	-22.44

Table 2.6

Variation of the level of the intense side lobe and the intensity at $\theta = 90^{\circ}$ for the 69 and 49-element array formats, for different angles of orientation between the crosses.

Angle between the crosses φ (in degrees)	69-element array		49-element array	
	Most intense side lobe level (in dB)	Intensity at 90° with respect to the reference elements (in dB)	Most intense side lobe level (in dB)	Intensity at 90° with respect to the reference elements (in dB)
15	-14.53	-14.53	- 9.56	-9.56
16	-16.15	-16.15	-10.34	-10.34
18	-16.76	-19.11	-11.81	-11.98
20	-17.45	-29.02	-12.71	-13.09
22	-17.75	-30.05	-13.59	-13.81
24	-16.13	-21.22	-14.37	-15.10
26	-15.03	-19.14	-14.69	-17.64
28	-14.52	-17.38	-14.26	-21.09
30	-14.56	-17.35	-14.18	-22.77
32	-15.08	-22.16	-14.46	-20.51
34	-16.04	-23.93	-15.05	-17.21
36	-17.34	-18.74	-14.76	-15.12
38	-17.65	-17.85	-14.41	-14.62
40	-18.09	-20.80	-15.48	-15.52
42	-17.88	-21.39	-15.59	-17.31
44	-16.98	-18.99	-14.96	-18.92
45	-16.85	-18.55	-14.83	-19.18

Table 2.7

A comparison of the beamwidths predicted by the nomograms with the calculated values.

Type of the array format	-3dB down point from the axis of the beam		-10dB down point from the axis of the beam		Intense side lobe level for the most favourable result (in dB)
	as per the nomogram (in degrees)	as per the calculation (in degrees)	as per the nomogram (in degrees)	as per the calculation (in degrees)	
43-element	3.0	2.8	5.2	4.90	-20.53
63-element	1.5	1.9	2.6	3.25	-19.59
45-element	3.0	2.8	5.2	4.9	-19.52
65-element	1.5	1.9	2.6	3.25	-22.90
47-element	3.0	2.8	5.2	5.0	-17.04
67-element	1.5	1.9	2.6	3.3	-19.70
49-element	3.0	2.8	5.2	5.1	-15.59
69-element	1.5	1.9	2.6	3.4	-17.75

with pressure release material or providing air gap of height $\lambda'/4$, where λ' is the wavelength of acoustic radiation in air, at the design frequency.

The advantage of the loosely packed array format is that closely packed planar arrays (CPPA), the elements of which are half-a-wavelength apart, can be converted to the proposed format, by selectively switching only those elements that produce the required beam pattern.

The results of the beam patterns for different array formats, given in tables 2.1, 2.4, 2.5 and 2.6 clearly emphasise the need for some sort of programmable switching system, to facilitate the switching of the desired format, as per the need, due to the fact that the angles of orientation φ are different for different formats, for the most favourable results.

2.5 Conclusion

The beam patterns were evaluated for different spacing, number of elements and different values of φ. Also, evaluations with slight changes in spacings, other than those correspond to the integral multiples of $\lambda/4$, were also attempted. The significant results of these evaluations were presented.

CHAPTER III

DEVELOPMENT OF A PROGRAMMABLE SWITCHING SYSTEM

3.1 Introduction

The beam patterns obtained from the theoretical analysis differ from those measured experimentally, due to the acoustic impedance variations of individual elements. The beam pattern can also be evaluated by the computation of acoustic impedances of individual elements with the help of suitable programs in a computer, which are readily available for circular and rectangular piston transducers [4a]. By inserting the actual acoustic impedance values, the beam pattern can be evaluated and further modifications to these patterns are made by adding or removing some elements, determined by their locations, by 'trial and error' method.

The time-consuming and tedious process of evaluating the acoustic impedances and then modifying the beam pattern, can suitably be replaced by a microprocessor based selective switching system for the elements, whose locations can be introduced in the form of certain instruction sets. An 8080 based switching system is developed to achieve this switching.

3.2 Hardware Description of the System

The processing unit contains an 8080 CPU group, 1702 EPROM, 2114 RAM, key board, 6-digits of 7-segment LED displays with the display circuits, decoding, latching and switching circuits, for the effective switching of the transducers. Presently, the system provides 1K bytes ROM and 2K bytes RAM areas with a provision for further expansion out side the board. A general purpose monitor is included in the ROM area 0 - FF to enable this system to serve as a general purpose processor.

Datas, in hex formats, used to control the transducers are fed into the system through the key board. The 7-segment LED displays are used to display the input data, memory address and memory data as judged by the key board operations.

A functional block diagram of the system is shown in Fig.3.1. The circuit diagrams of the CPU module, the memory module, display unit, and decoding unit are shown in Figs. 3.2, 3.3, 3.4 and 3.5, respectively. The circuit diagram of the latching unit, incorporating 32 transducer elements, is shown in Fig.A.II.1.

The output signal conditions, appearing at the different output port terminals as per the commands to the

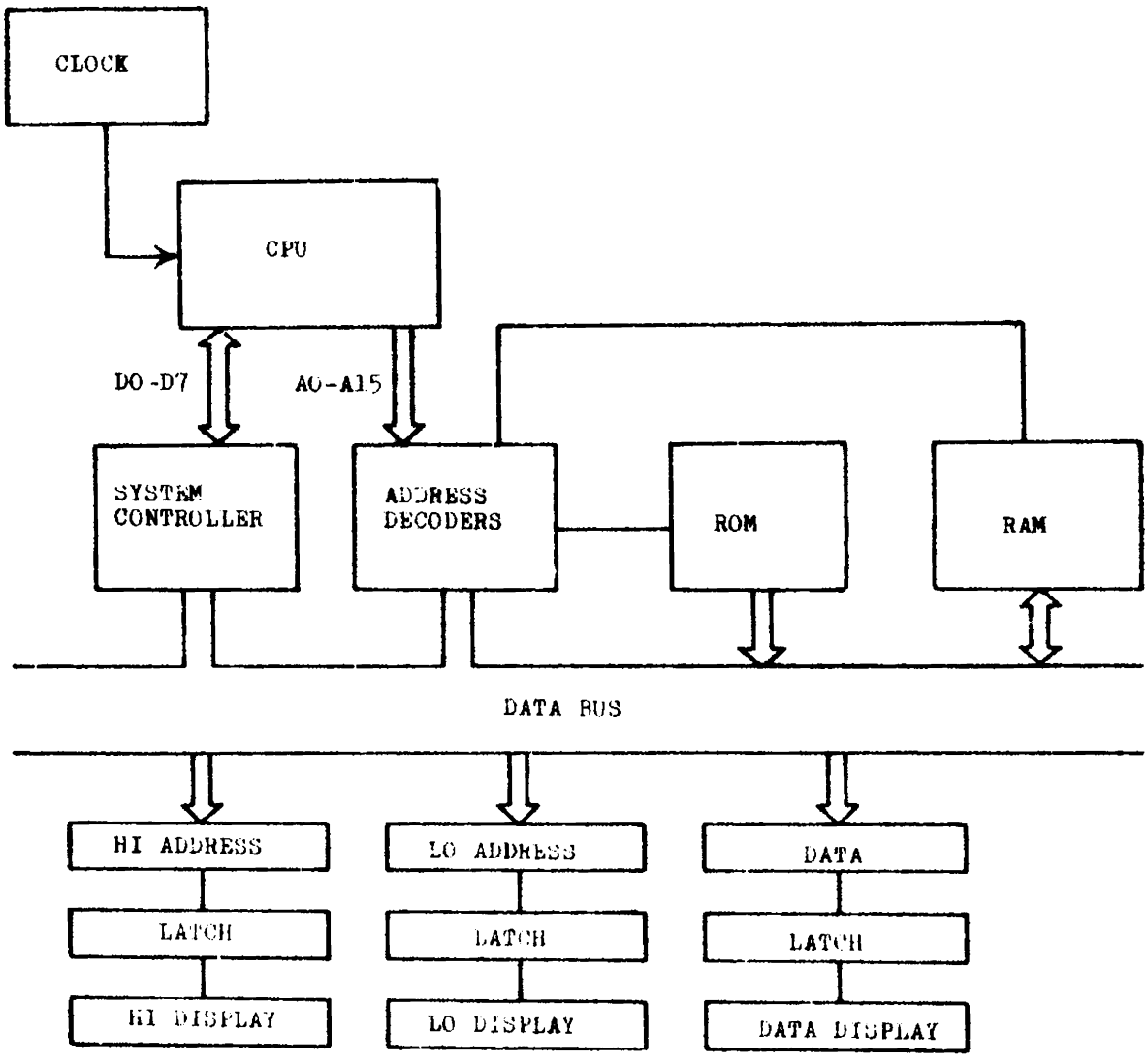

Fig.5.1: BLOCK DIAGRAM OF THE SWITCHING SYSTEM

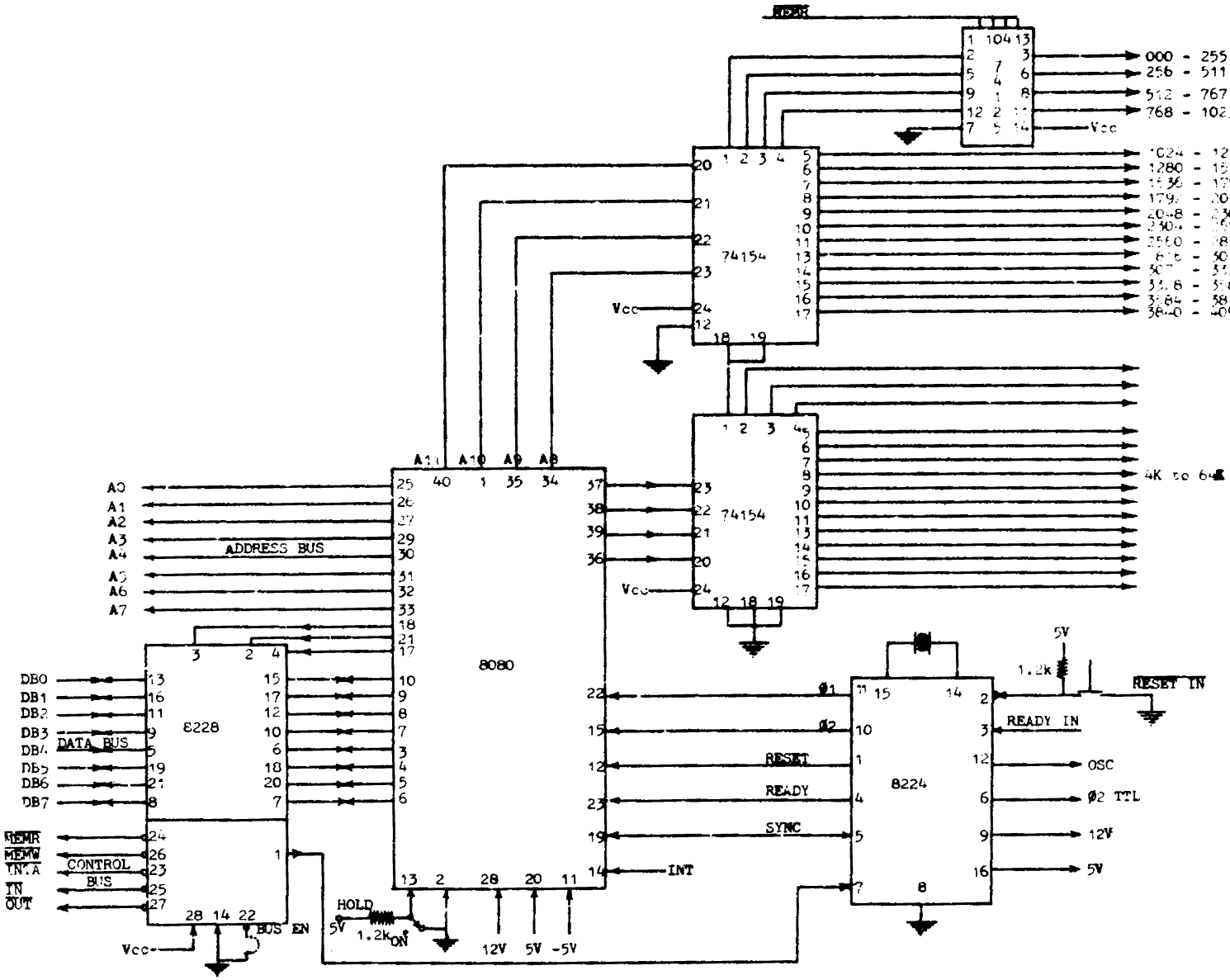

Fig. 3.2: CIRCUIT DIAGRAM OF THE CPU MODULE

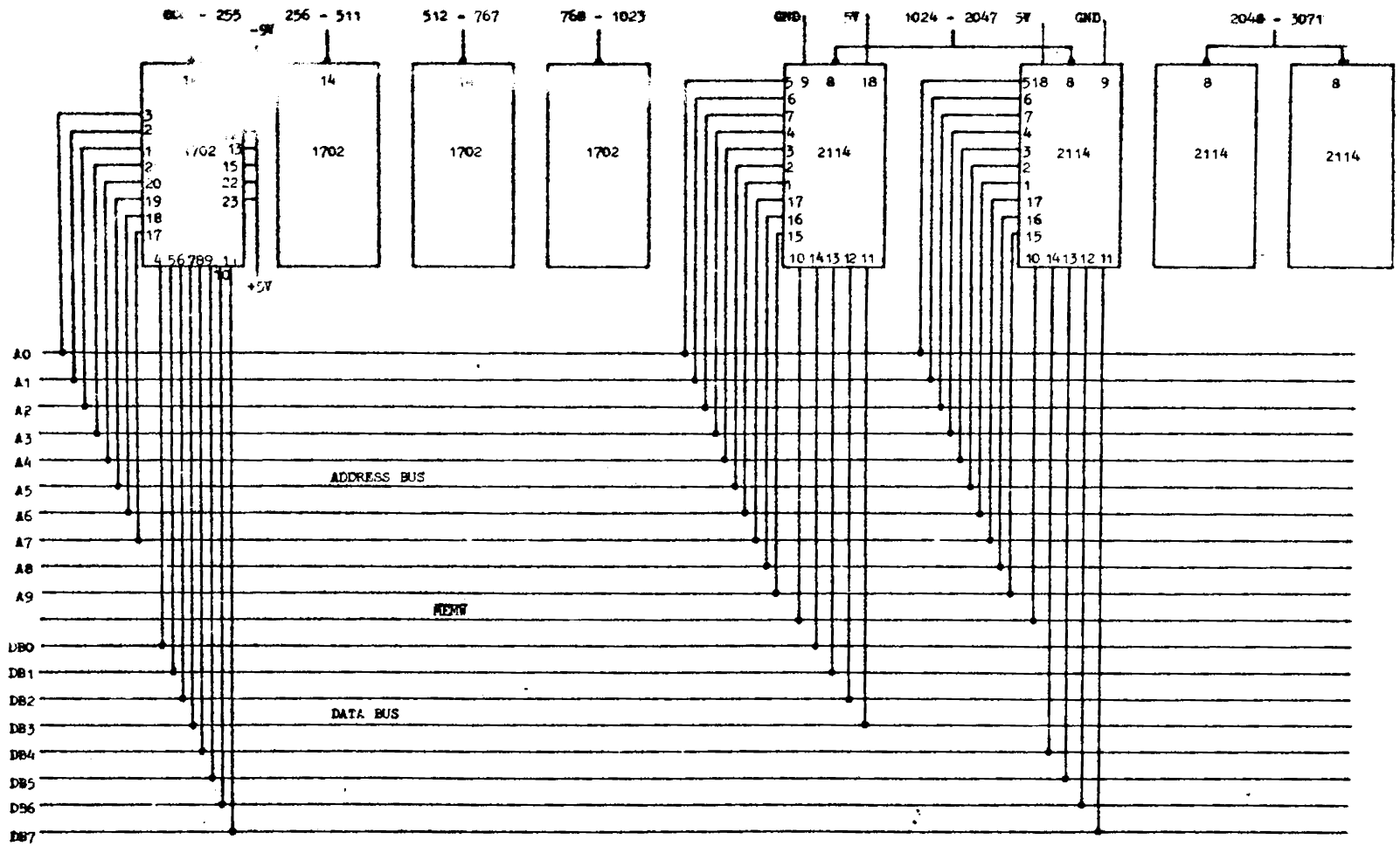

Fig.3.3 : CIRCUIT DIAGRAM OF THE MEMORY MODULE

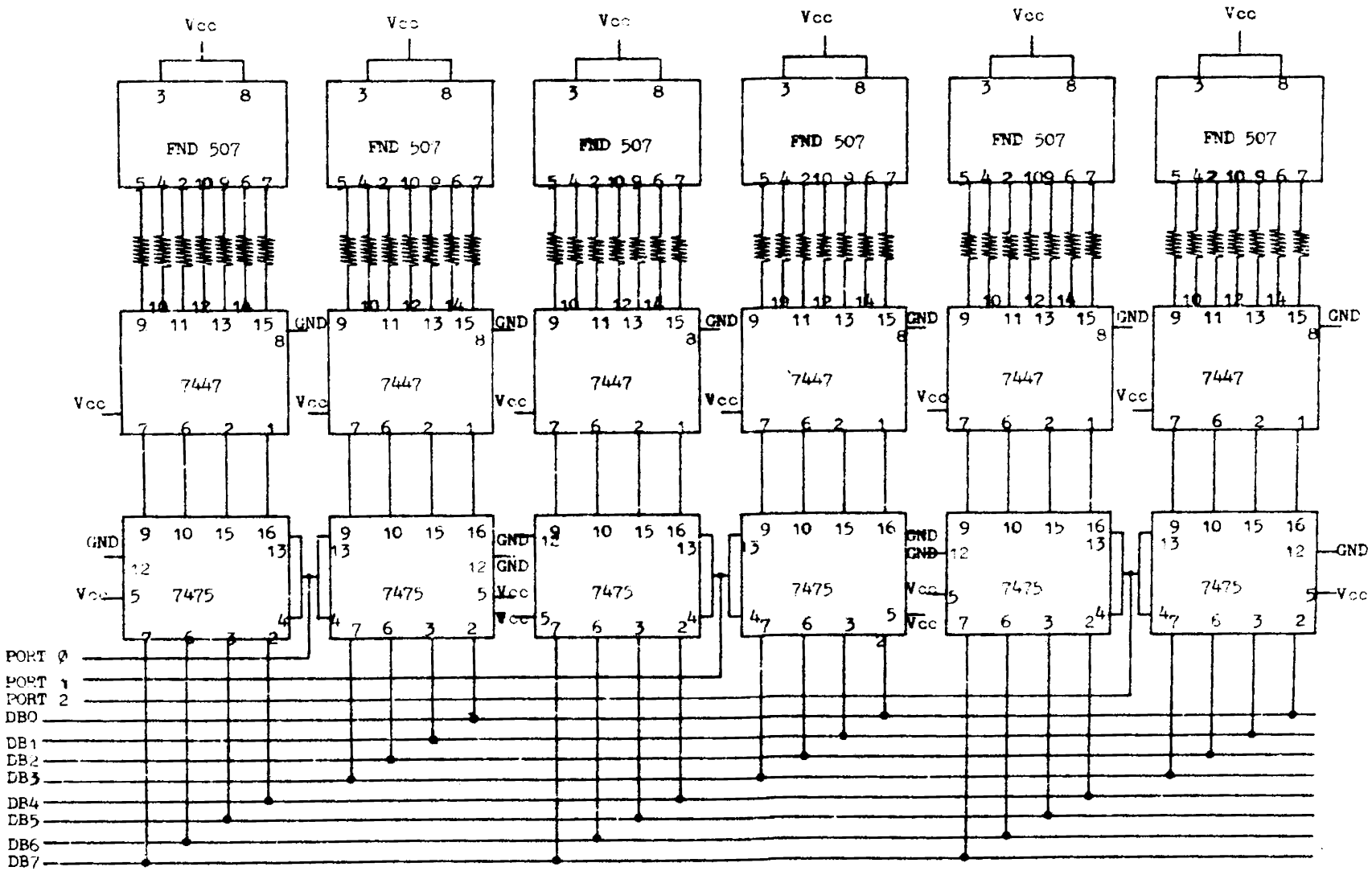

Fig.3.4: CIRCUIT DIAGRAM OF THE DISPLAY UNIT

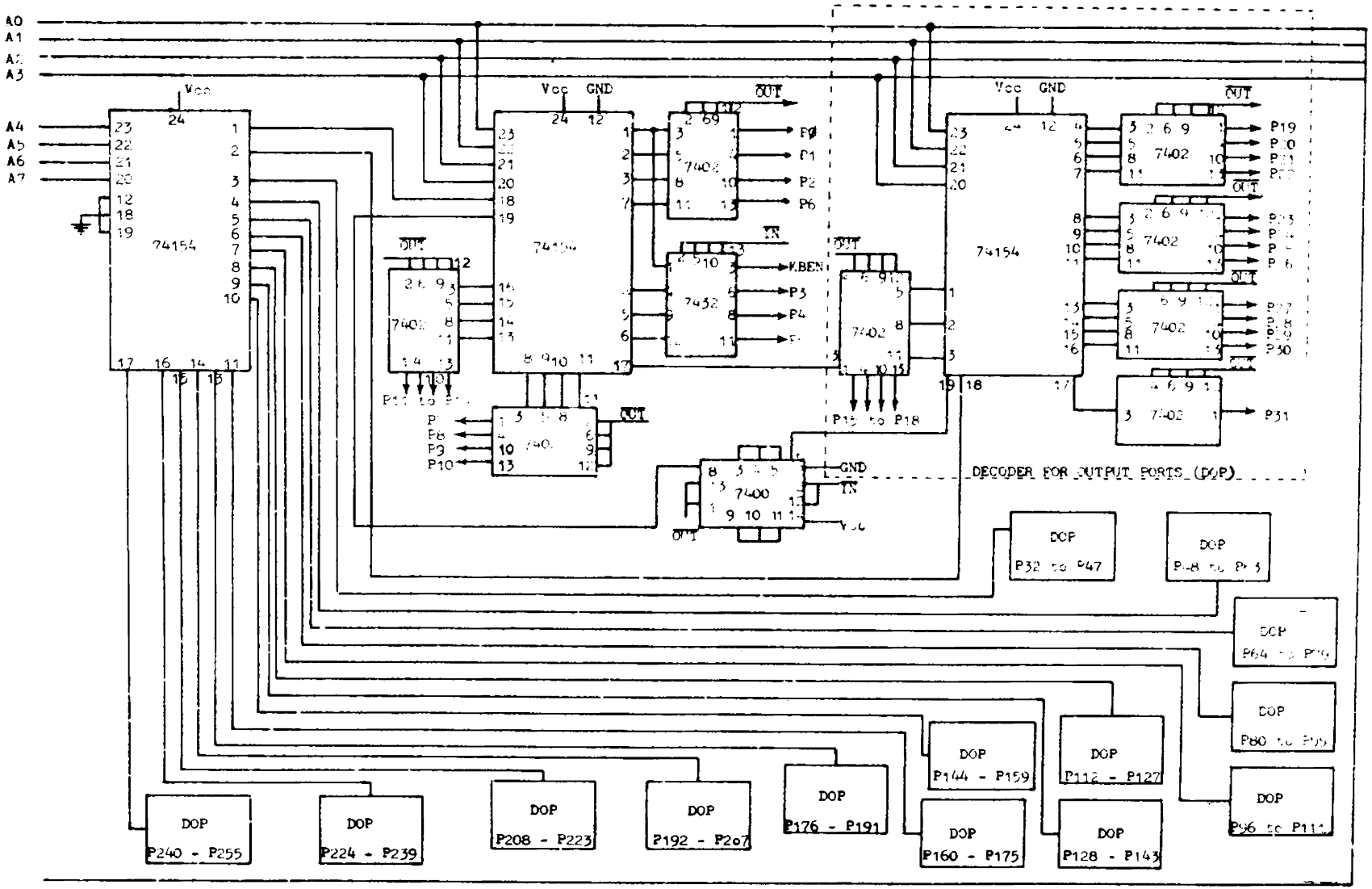

Fig.3.5: CIRCUIT DIAGRAM OF THE DECODING UNIT

CPU are used to latch the data in the latching unit which control the respective transducer, through the associated transistor and relays as shown in Fig.3.6.

The external view of the switching system and the stacked view of the various modules of the system are shown in the photographs of Fig.3.7 and Fig. 3.8, respectively. Figs. 3.8(i) and 3.8(ii) are the top view and front view of the stacking.

3.3 Software Description

The addresses of the read memory and read/write memory are :

00, 00	TO	03, FF
	and	
04, 00	TO	0B, FF

respectively. Memory locations other than those defined are not used in the switching system and are blank areas.

Presently, the system can be used to control 256 transducer elements through 32 output ports.

3.4 Selective Switching - An Illustration

As an illustration, consider a CPPA with 32 transducer elements, which are controlled through Port 06,

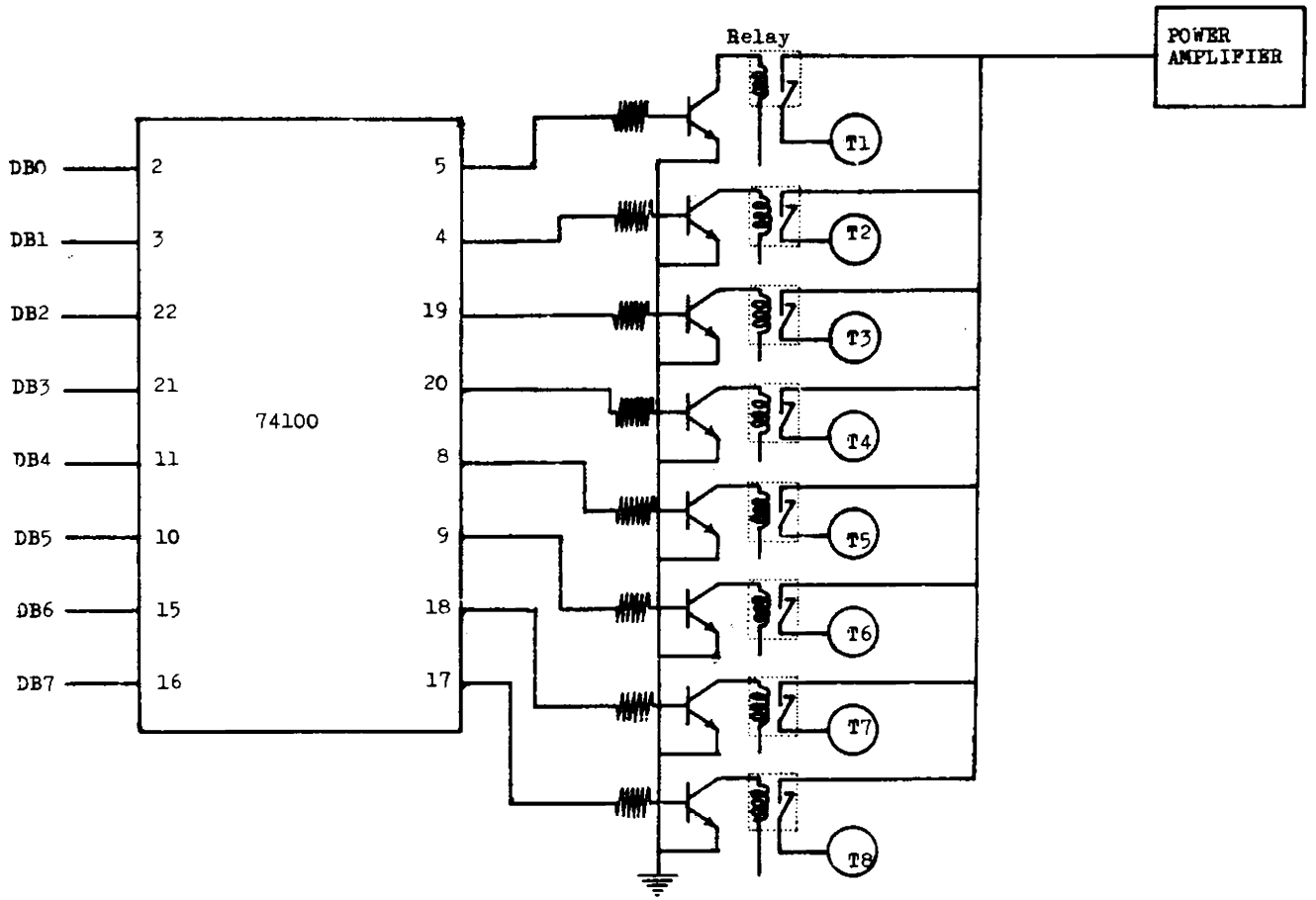

Fig.3.6 : An illustration of the switching of 8 transducers using the switching system

Fig.3.7: External view of the Switching System

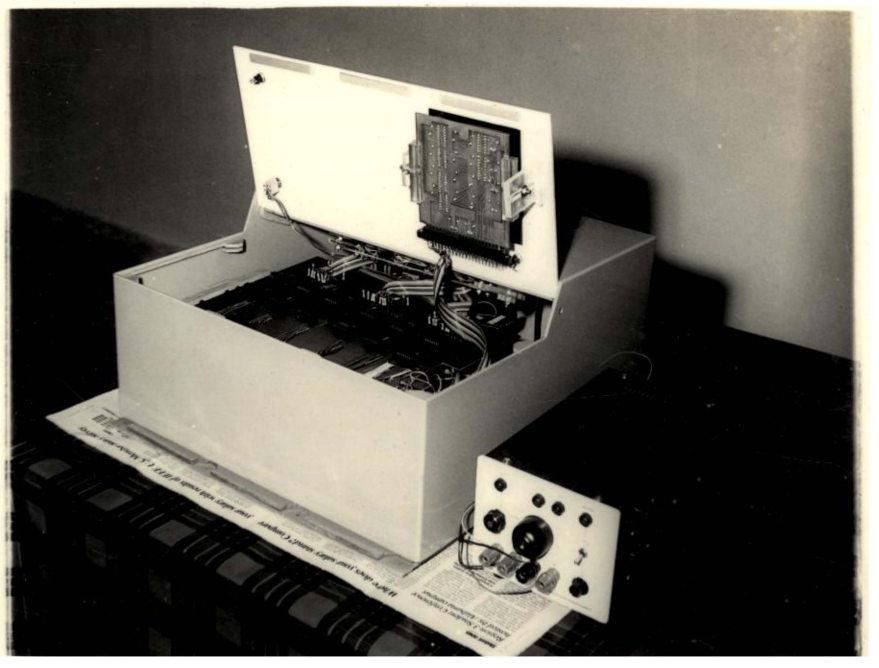

Fig.3.8(i): Top view of the stack of various modules

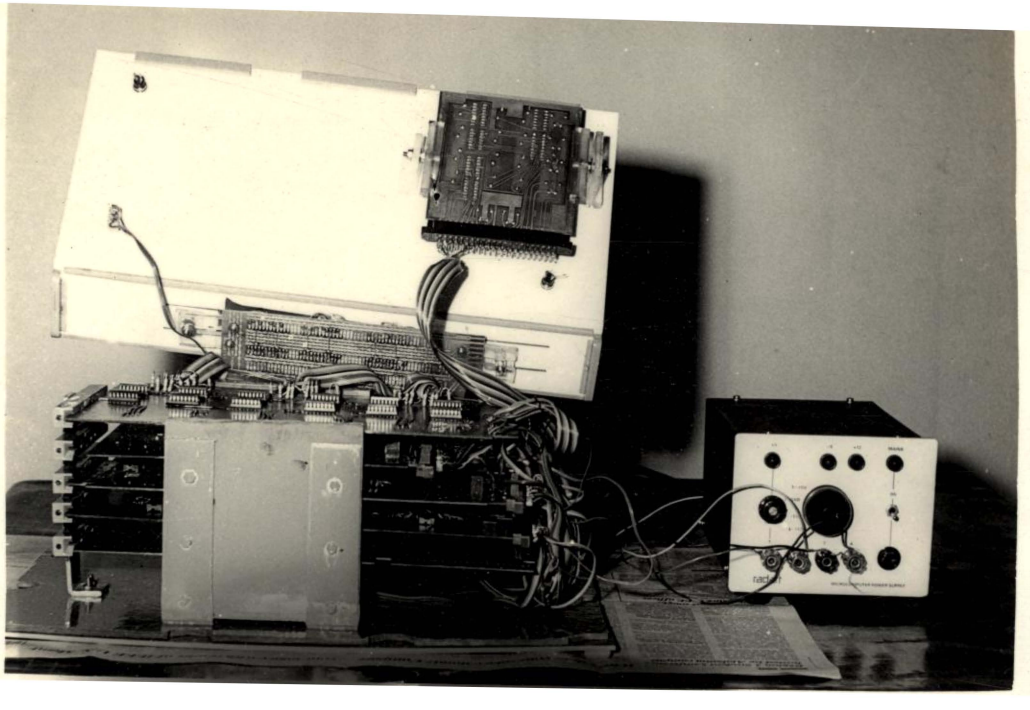

Fig.3.8(ii): Front view of the stack of various modules

Port 07, Port 08 and Port 09, as shown in Fig. A.II.1. The flow chart and the program for switching T1, T2, T7, T8, T9, T11, T14, T16, T19, T20, T23, T25, T27, T29 and T31 is given in Appendix III.

3.5 Conclusion

The switching system described here can be effectively utilised for developing narrow beam arrays by selectively switching those elements, that produce the required beam pattern, from the closely packed plane circular array. Once a favourable beam pattern is achieved by this technique, light arrays can be fabricated at the economy of transducer elements.

CHAPTER IV

DEVELOPMENT OF PROGRAMMABLE ARRAYS

4.1 Introduction

The LPA format discussed in chapter II suffers from the following drawbacks, when compared to a CPPA.

1. Low array gain, due to the limited number of elements, which limits its usefulness under conditions of low signal-to-noise ratio. But it can be effectively used under conditions of high signal-to-noise ratio where the array gain is immaterial and factors like weight, cost and directionality are important.
2. Lobe switching is not possible and
3. Amplitude shading cannot be employed without the use of additional hardware.

The design of a programmable array, with modifications to offset these drawbacks, using the switching system in conjunction with a CPPA is presented in this chapter.

For the measurements under conditions of low signal-to-noise ratio, a higher array gain, if necessary,

can be obtained by exciting all the elements of the CPPA. Though, the LPA format, presented in chapter II, is basically an unshaded one, it can be shaded for reducing the side lobe levels still further, with the help of the switching system, at the cost of further reduction in array sensitivity. Amplitude shading [39] can be realised by a technique known as, 'Shading by an Average Amplitude in Time'('SAAT'). Also, lobe switching can be accomplished by switching those elements of the CPPA, depending on the region to be insonified. Thus depending on the purpose, for which the array is intended, any of these techniques can be employed on a CPPA, to get the desired array format.

4.2 Shading by an Average Amplitude in Time

Consider a CPPA, with a uniform element spacing of $\lambda/2$, where λ is the wavelength of acoustic radiation at the design frequency. By selectively switching the elements as per the scheme discussed in chapter II, using the switching system described in chapter III, an LPA results. By judiciously switching the elements 'with reference to time', amplitude shading can be realised. Thus the switching system can also be used for shading by an average amplitude in time. The switching for the required shading can be accomplished by suitable programs.

The arguments which support the SAAT operation are,

1. The signal frequency employed for ranging and other propagation type of uses is very low, when compared to the system clock.
2. The propagation velocity of acoustic radiation is low.
3. Echo-ranging measurements are normally taken once in every 2.5 ms or so which is large when compared to the switching speed.
4. The mode of propagation of acoustic energy is longitudinal in nature.
5. There are multi-path propagations.
6. Transducers employed are of narrow-band type, thereby eliminating the modulation terms that may arise due to acoustic interactions and due to pulsed operation.
7. The medium is low-pass and it provides certain amount of averaging.

Therefore, it is possible to control the individual element response on an average amplitude basis, rather than on an absolute amplitude basis. Since the signal generator is only being gated, the radiated signal is coherent and

hence the SAAT will provide a true average rather than a random average, leading to an effectively shaded array.

4.3 Timing Considerations for the SAAT

The timings that control the effectiveness of the SAAT operation are,

1. Timing of the radiated signal involved with respect to the measurement time.
2. Timing of the output switching.

These timings should be properly selected so as to get the desired averaging effect and hence the required shading formula.

A typical calculation for the SAAT timing is given below.

Consider an array used for ranging sonar.

Let the frequency used be 20kHz.

The cycle time of the radiating signal will be 50μs

Let the range measurements be taken in every 5ms.

The beam formed by the array settles to an average in 50μs.

The ratio between the measurement time and averaging time is

$$\frac{5\ \text{ms}}{50\mu\text{s}} = 100$$

This is a very good value, for the SAAT operation.

4.4 Specific Examples for the SAAT Operation

4.4.1 Binomial Shading

In binomial shading, the amplitude distributions of various elements of a 6-element array should follow the shading formula 0.1, 0.5, 1, 1, 0.5 and 0.1. The output switching times for different elements T1, T2, T3, T4, T5 and T6 are shown in Fig.4.1.

4.4.2 Dolph-Chebyshev Shading

The shading formula for a 6-element line array, obeying the Dolph-Chebyshev distribution is 0.30, 0.69, 1, 1, 0.69 and 0.30. Fig. 4.2 illustrates the output switching times for this type of distribution.

4.4.3 Continuous Distribution Shading

A 5-element linear array, shaded on the continuous distribution basis follow the shading formula 0.4, 0.8, 1, 0.8 and 0.4. Fig. 4.3 illustrates the output switching time durations for different elements.

In these specific examples, the shaded regions of Figs. 4.1, 4.2 and 4.3 represent the ON time while the vacant regions, if any, represent the OFF time of various elements.

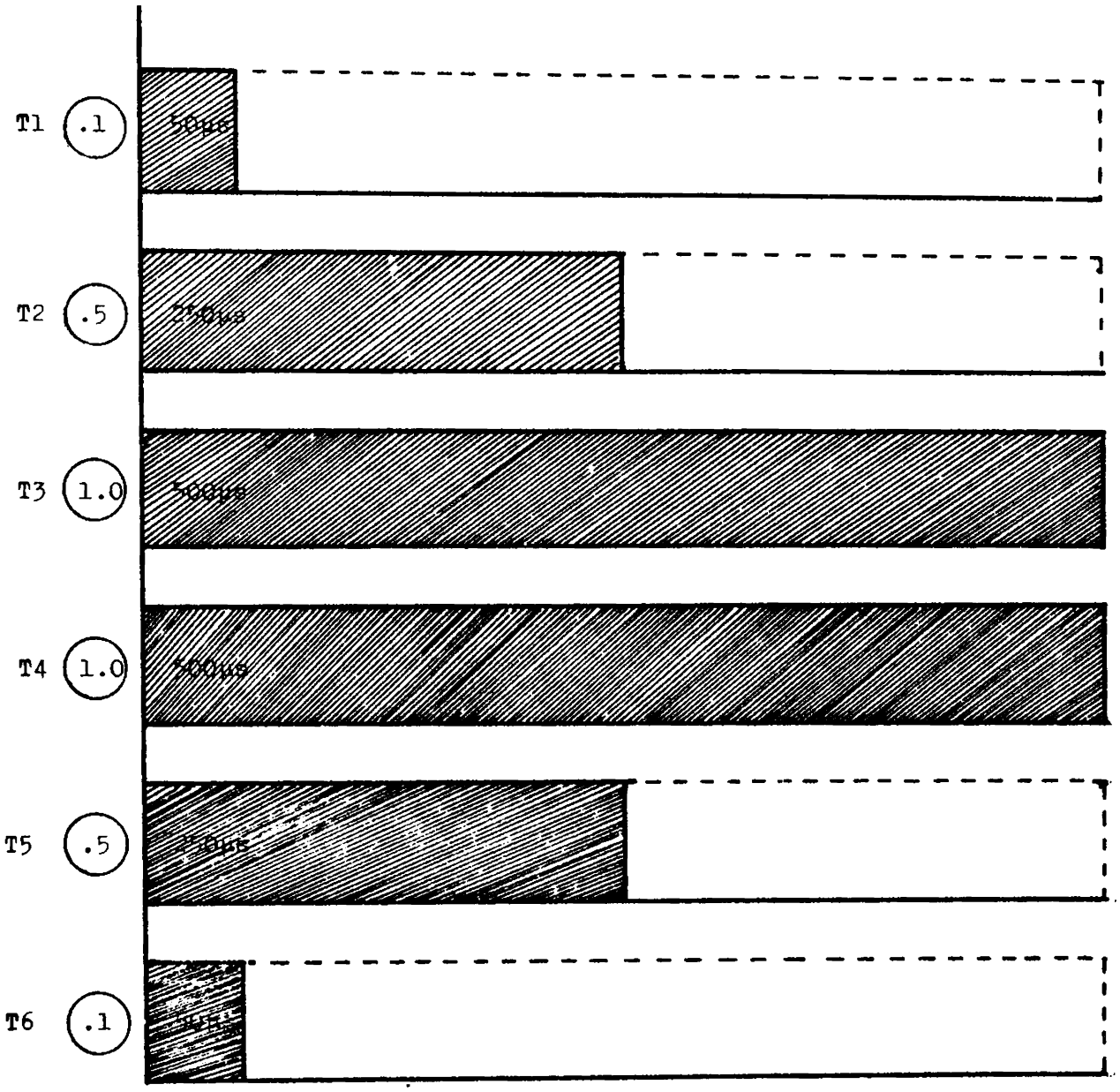

Fig.4.1 : Illustration of the output switching time durations for different elements of a 6-element linear array for the Binomial Shading

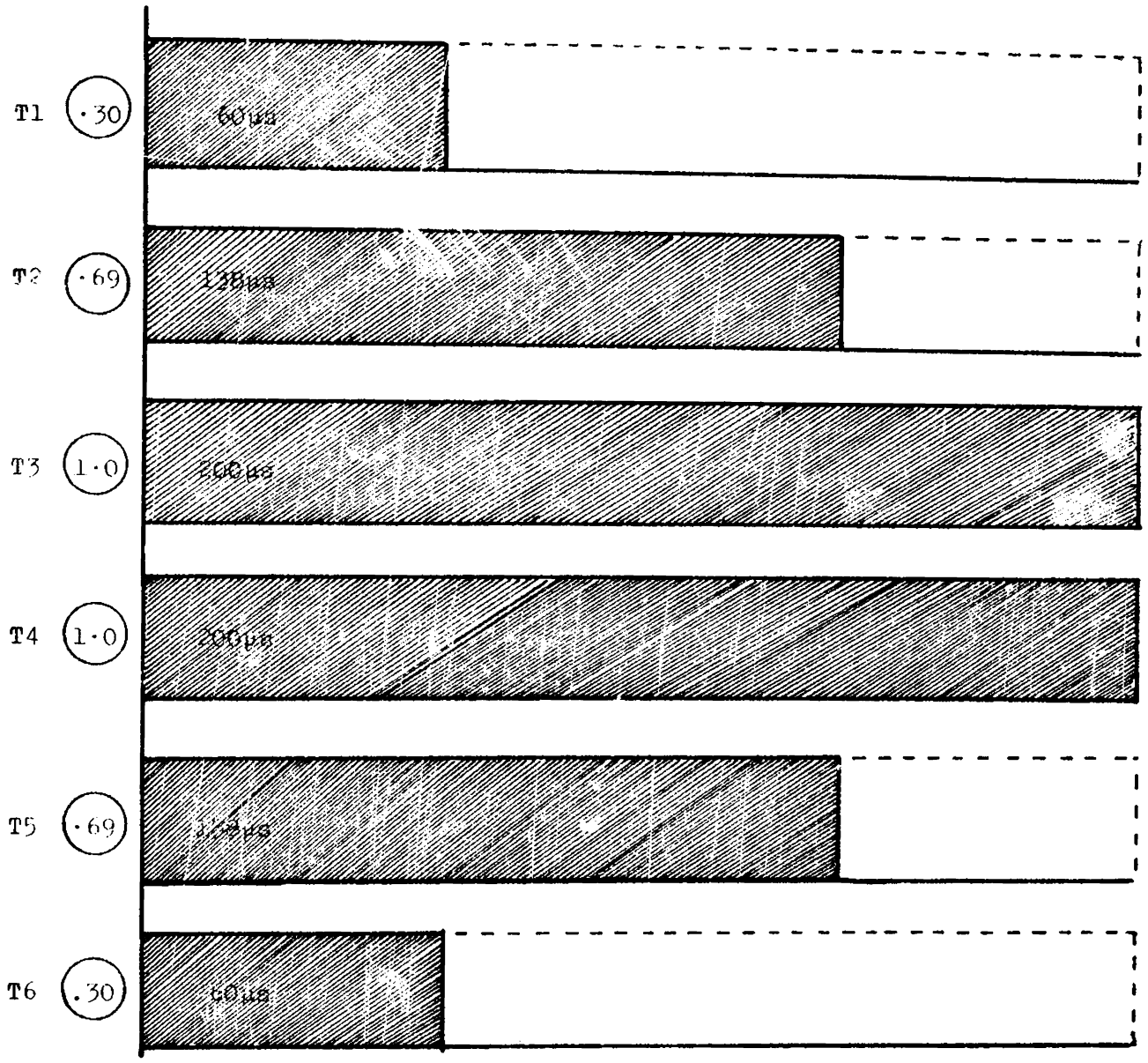

Fig.4.2 : Illustration of the output switching time durations for different elements of a 6-element linear array for the Dolph-Chebyshev Shading

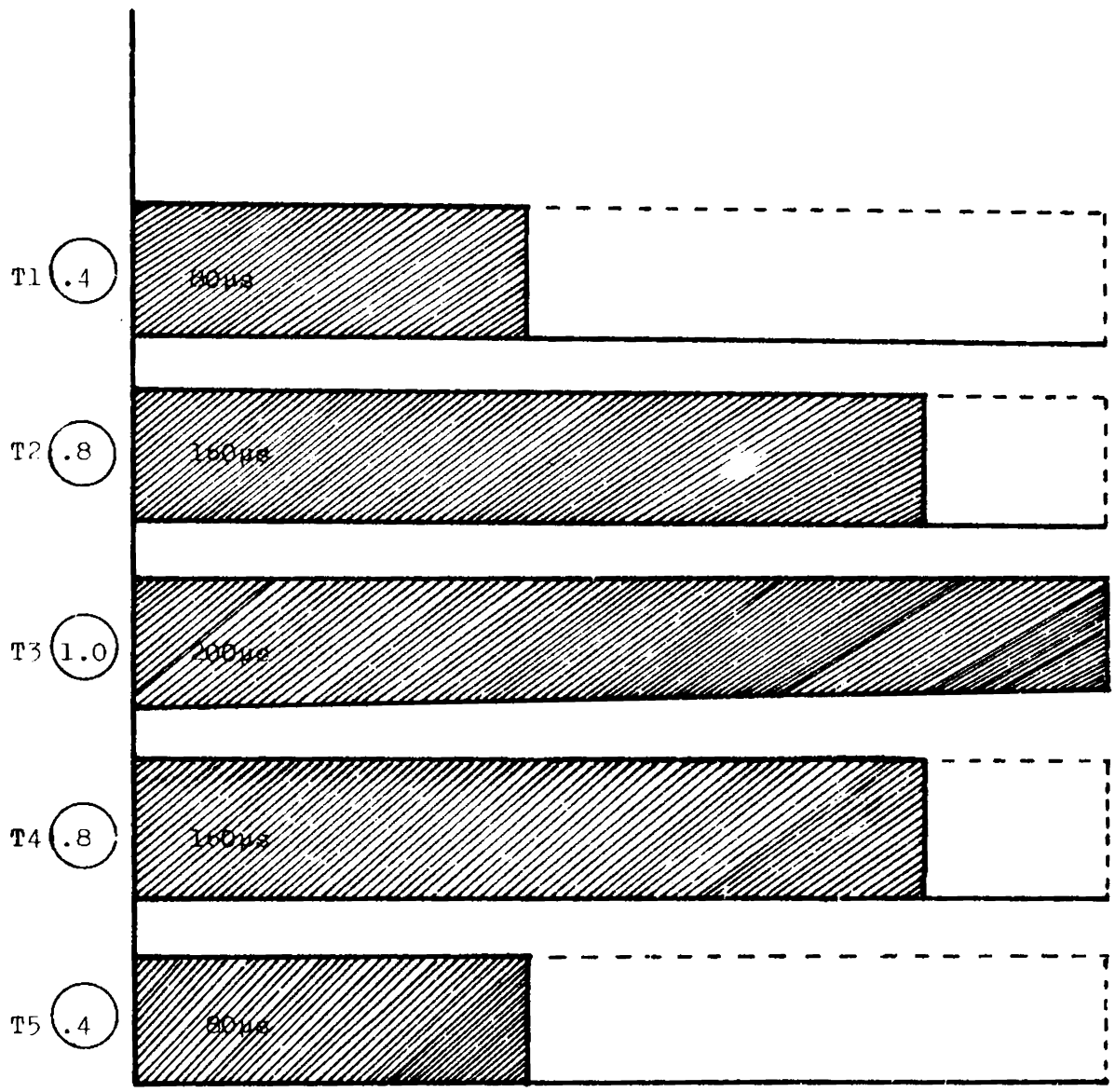

Fig.4.3 : Illustration of the output switching time durations for various elements of a 5-element linear array for the continuous Distribution Shading

In an analogous manner, any shading formula can be employed or verified, by suitably controlling the switching times. The flow charts and the programs for the output switching time control for the above three specific examples, for arrays operating at 20kHz, are given in appendix IV. The timings for the switching program are evaluated for a clock period of 0.5 μs.

4.5 Comments on Spurious Frequencies due to Switching

SAAT switching will generate spurious frequencies. The effects of these new frequencies on the operating frequencies are listed below.

1. The frequencies that are generated due to switching will be larger when compared with the operating frequency and hence they get attenuated easily.
2. The envelope itself might form a shading. However, the various parts of the envelope are noncoherent and hence there is no danger of a spurious beam at the envelope frequency being developed.
3. The intermodulation between the envelope and the radiating frequency will be negligible, even though the medium is nonlinear.

4.6 Comments on SAAT Operation

The SAAT technique can be successfully implemented for hydrophone arrays as well. The beam switching and different pattern generations can be realised in very short times, of the order of 0.5 ms.

The relay switching, discussed in chapter III, cannot be successfully implemented for the SAAT operation, due to their operate and release time lags. For effective and efficient switching, semiconductor devices may be adopted.

4.7 Conclusion

It has been demonstrated that various time durations can be introduced by the software technique. Hardware techniques will accomplish this purpose by setting the potentiometers, control switches etc. The switching system can be properly programmed to insert the required ON/OFF time durations in any element.

The concept of amplitude shading on an average amplitude basis rather than on an absolute amplitude basis can be shown to be practicable. Similarly placing of nulls and switching of main lobes can also be accomplished by programs. Thus all the disadvantages imposed by the LPA format can be rectified by suitably implementing

the CPPA in conjunction with the switching system, as per the need. Also, any shading mechanism and any form of lobe switching can be achieved simply by calling the addresses of the particular program loaded in the read memory area of the switching system, without changing the array, as a whole or without physically moving it.

Though the illustrations for the specific examples are undertaken for a linear array, it can be extended to an LPA or CPPA format.

CHAPTER V

APPLICATION OF THE LPA FORMAT

5.1 Introduction

The application of the LPA format towards nonlinearity study is discussed in this chapter. Nonlinearity in 'underwater acoustics' appears in various forms. It causes the effect of cavitation, distorts an initially sinusoidal sound wave to a saw tooth form etc.

The LPA format proposed in chapter II, which conforms to the suggestion of Carson, is capable of producing narrow beams at the difference frequency due to the nonlinear interactions between the two primary frequencies, besides reducing the interaction effects among the radiators, due to its finite radiating aperture.

5.2 Application Towards Nonlinearity Study

One of the most important effects caused by the nonlinearity is the dependence of the propagation velocity on the pressure amplitude. This dependence can be explained in terms of the bulk modulus and density. In basic acoustic theory of propagation, certain approximations were made to avoid the complexity in the analysis.

This approximation is valid only for small amplitudes of the acoustic signal. Hence, if the amplitude is small, the nonlinear effect is small and its neglect is justifiable. If the wave amplitude is large, nonlinear effects become significantly large [3c],[23].

Due to the dependence of the propagation velocity on the pressure amplitude, a sinusoidal wave form transforms to a saw-tooth like as it propagates, having a steep beginning and a sloping tail. This is explained as being due to the generation of the harmonics of the fundamental frequency.

In any nonlinear medium, for example in water, if two acoustic radiations at frequencies f_1 and f_2 are allowed to propagate in the same direction, they will interact, giving rise to the sum and difference frequencies, along with the primaries. If the primary frequencies are high, they get easily absorbed along with the sum frequency component. The difference frequency component can be advantageously utilised for carrying out secure communications [3c],[20]. The amplitude of the nonlinearly generated difference frequency signal will continually increase with distance from the projector and beyond a certain distance, the amplitude of the difference frequency signal starts to decrease [22],[23].

The generation and transmission of low frequency acoustic waves is a difficult process due to the need for large size transducer elements. However, the nonlinear interaction between two acoustic radiations will generate the difference frequency signal, which can fall in the low frequency zone of the spectrum, depending on the primary frequencies. The advantages of the nonlinearly generated low frequency sound waves, over its direct launching, will offset the inefficient conversion mechanism involved in the process.

The problem of sound scattered by sound was investigated by Berktay [27], Al-Temimi [27] and Westervelt [35]. Experimental results found in literature [20], show that narrow beams at the difference frequency can be generated even with transducers of small radiating aperture.

According to the theoretical analysis [20],[40], on the difference frequency generation, the two dimensional directivity pattern contains an aperture term, which for finite apertures, where the aperture area S is larger when compared to the square of wavelength of acoustic radiation at the difference frequency, is significant. The larger the value of S, the smaller will be the half power beamwidth. The directivity pattern of the difference frequency signal is,

$$D(\theta') = \frac{A_f}{\sqrt{\left\{1 + \left[\frac{2K'}{A'} \sin^2 (\theta'/2)\right]^2\right\}}} \qquad (5.1)$$

where

A_f = the aperture factor

θ' = the angle which the observer makes with the acoustic axis

$A' = \alpha_1 + \alpha_2 - \alpha' \cos \theta'$

α_1 and α_2 being the absorption coefficients of the primary frequencies f_1 and f_2, respectively and α' that of the difference frequency.

$K' = \frac{2\pi}{\lambda''}$

the wave number at the difference frequency, λ'' being the wavelength of acoustic radiation at the difference frequency.

The radiating aperture of the 43-element LPA format is almost circular. Since the diameter of its radiating aperture is 10λ, λ being the wavelength of the primary frequency, the influence of the aperture term on the directivity pattern cannot be neglected.

The form of the aperture factor for circular radiating apertures will be

$$A_f = \frac{2J_1(aK' \sin \theta')}{(aK' \sin \theta')} \qquad (5.2)$$

where

$J_1 (aK' \sin \theta')$ = the first order Bessel function of argument $(aK' \sin \theta')$,

a being the radius of the aperture of the array.

If the area of the aperture is large, then the aperture factor will have a prominent role in the HPBW. Thus by making the aperture very large, the HPBW at the difference frequency can be made smaller.

In the 43-element LPA format, the aperture area is made very large with limited number of transducer elements, thereby reducing the beam width at the difference frequency. Also, by exciting alternate elements of the LPA with the two primary frequencies f_1 and f_2, the chance of interaction is increased, thereby reducing the length of the interaction column.

The following examples illustrate the influence of the aperture term on the directivity pattern.

Let $\frac{1}{2}(f_1 + f_2)$ = 20 kHz and

$f_1 - f_2$ = 3 kHz

Radius of the array, = 37.5 cms

Wavelength at the difference frequency = 50cms

In this case, the aperture area $S >> \lambda^2$

Hence the aperture term is significant. The directivity patterns with and without the aperture terms are shown in Fig.5.1. The full line and dotted line drawings, respectively, represent the patterns with and without the aperture term.

Similarly, corresponding to

$\frac{1}{2}(f_1 + f_2)$ = 100 kHz and

$(f_1 - f_2)$ = 15 kHz,

the directivity patterns with and without the aperture terms are, shown in Fig.5.2.

It can be seen that the aperture factor influences the directivity pattern very much, from 15^o onwards, where the intensity level is too small with reference to the lobe intensity. But, if the difference between

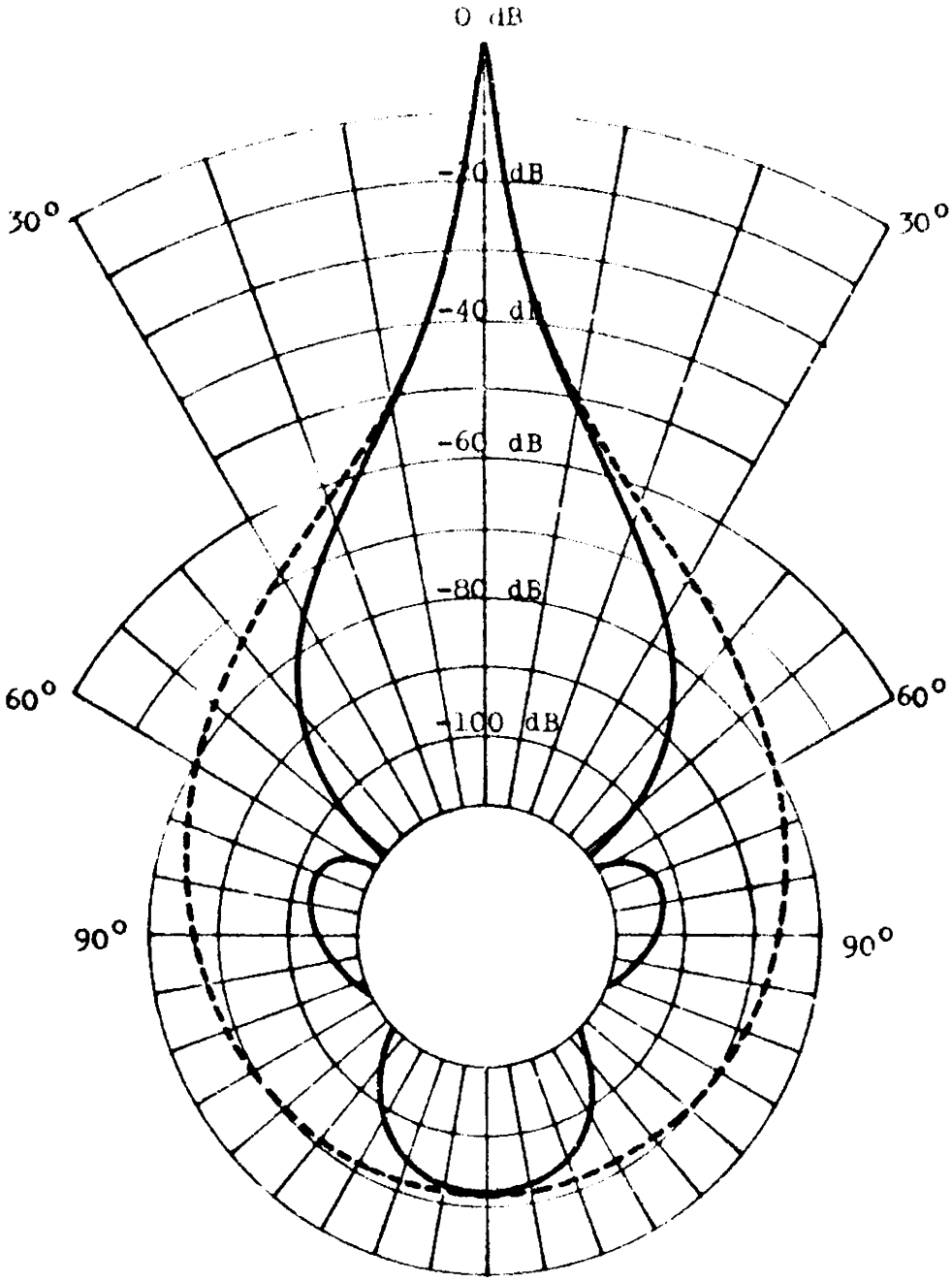

Fig.5.1 : Directivity patterns with and without the aperture term for 3 kHz difference frequency signal (Full line and dotted line drawings, respectively represent the patterns with and without the aperture term)

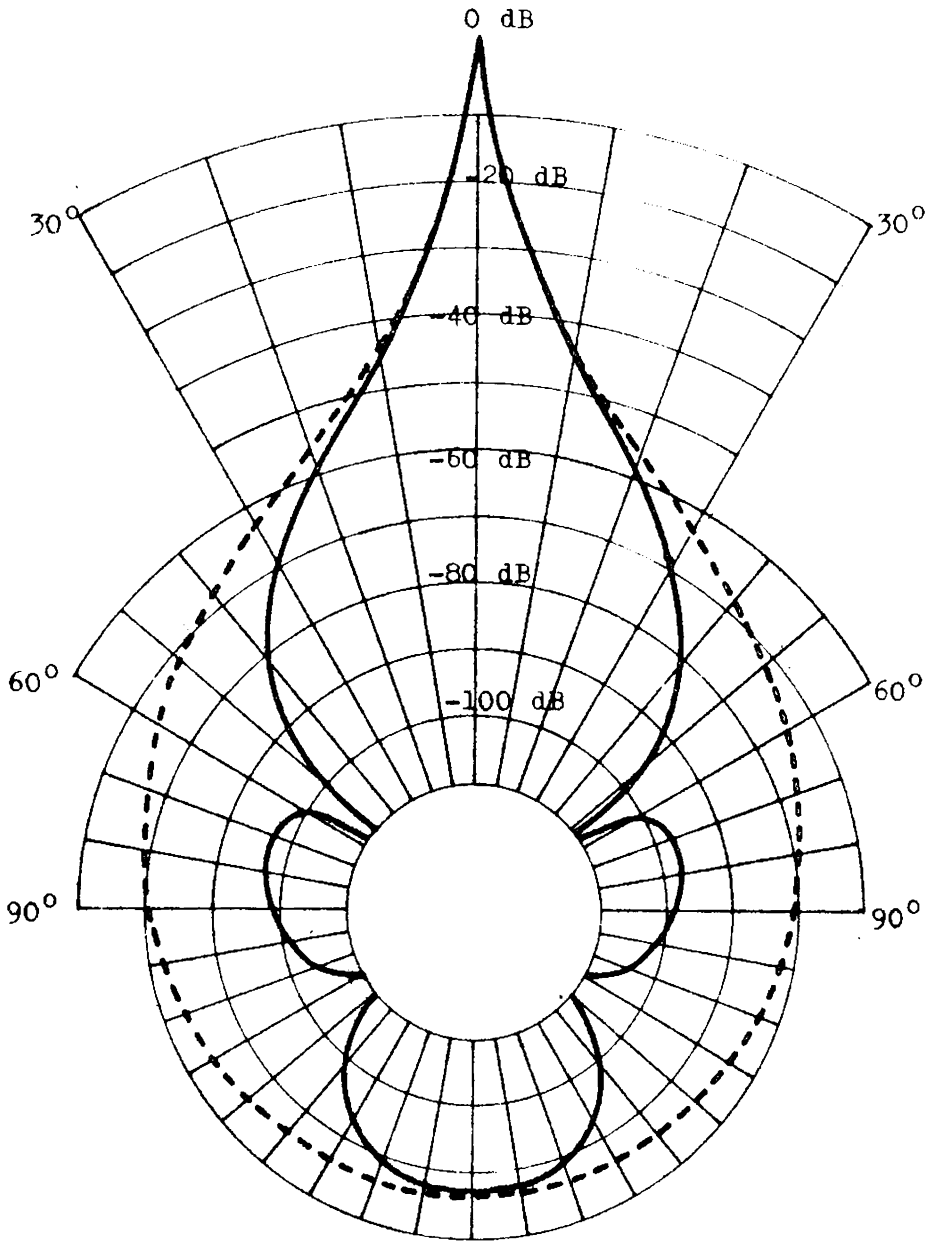

Fig.5.2 : Directivity patterns with and without the aperture term for 15 kHz difference frequency signal

f_1 and f_2 is increased, the effect of the aperture term becomes very much pronounced in the lobe direction and hence the intensity in this direction falls quickly. Computer evaluations, in this favour, yielded wrong results, basically due to the approximations made in the system in terms containing higher powers of $(aK' \sin \theta')$, during the evaluation of the Bessel function.

The theoretical prediction of the actual impact of the finite radiating aperture of the 63-element array on its difference frequency directivity pattern cannot be made due to the departure of its aperture geometry from that of the 43-element one. However, it can be concluded that, the beam widths at the difference frequency radiation will be less than that of the 43-element array.

Though, it was intended to study the usefulness of the LPA format towards cavitation effect, it has not been possible to investigate the idea to acceptable levels of accuracy.

5.3 Conclusion

Application of the LPA format towards the generation of narrow beam low frequency sound waves through nonlinear interactions is proposed. The nonlinearly generated low frequency signal has certain attractive operational features over the direct launching of such a signal into water.

CHAPTER VI

FINITE MEDIUM EFFECTS ON TRANSDUCERS

6.1 Introduction

Ceramic transducer elements used for underwater propagation applications have a metallic radiating face, coupled to the ceramics. Usually, these transducer elements are either immersed in a container of insulating fluid or moulded in rubber so as to insulate them from water, during direct water loading experiments. If the transducer is enclosed in a container of fluid, the radiation will be coupled to the medium through acoustically transparent rubber diaphragms. However, these acoustically transparent diaphragms cause small reflections whose effects are not negligible. They influence the performance characteristics of the transducer, such as its resonance frequency, impedance at resonance, the Q-factor, the efficiency of radiation and the related parameters.

Investigations on the effects of finite media on the performance of transducers were carried out. The finite medium was simulated by enclosing the transducer element in a semi-rigid container, filled with castor oil. This assembly was immersed in an acoustic test tank of

dimensions 12m x 8m x 6m, with slanting walls designed to avoid standing wave system. Results of these investigations proved that the signal which was reflected from the bottom and the sides of the container influenced the performance of the transducer, to a great extent.

Almost periodic variations in resonance frequency, impedance at resonance, the Q-factor and the efficiency of radiation were exhibited with change in depth of immersion of the radiating face of the transducer. It is to be pointed out that an approximately similar variation of impedance of magnetostrictive transducer elements is reported in [36]. It is felt that the experimental results presented in this chapter will be of more use than those reported in [36], because the latter reported an impedance variation at a frequency which corresponds to either the free-field or a constant-field condition. Experimentally, it is observed that the resonance frequency of a ceramic transducer element is affected by its depth of immersion in a finite medium. Keeping in mind this resonance frequency variation, with change in depth of immersion, an impedance variation at resonance is presented here. Starting from the differential equation governing the vibration of a transducer, the experimentally observed variations of resonance frequency, impedance at resonance, Q-factor and the efficiency of

radiation are explained in appendix V, where it is shown that the existence of the reflected signal, mainly from the bottom of the container, is responsible for this behaviour.

In these experiments, to realise an effectively large value of resistance, castor oil was taken as the fluid in the container.

6.2 Experimental Set-up and Results

The experimental set-up of the projector assembly, used to investigate the variations of resonance frequency and impedance at resonance is shown in Fig.6.1. The transducer element used in the projector assembly is fitted with a metallic cover, to insulate it from water during direct water-loading experiments. A rubber 'O' ring was attached to this cover for fixing it loosely to the radiating face, besides making it water-tight. The experiment consisted of the measurement of resonance frequency, impedance at resonance and the efficiency of radiation, exhibited by the ceramic transducer element, freely suspended at various depths. Measurements were made at every 5 mm depth of immersion of the radiating face, starting from the surface of the fluid, for various transducers. Figs. 6.2 and 6.3 respectively show the variations of resonance frequency and impedance at resonance, with

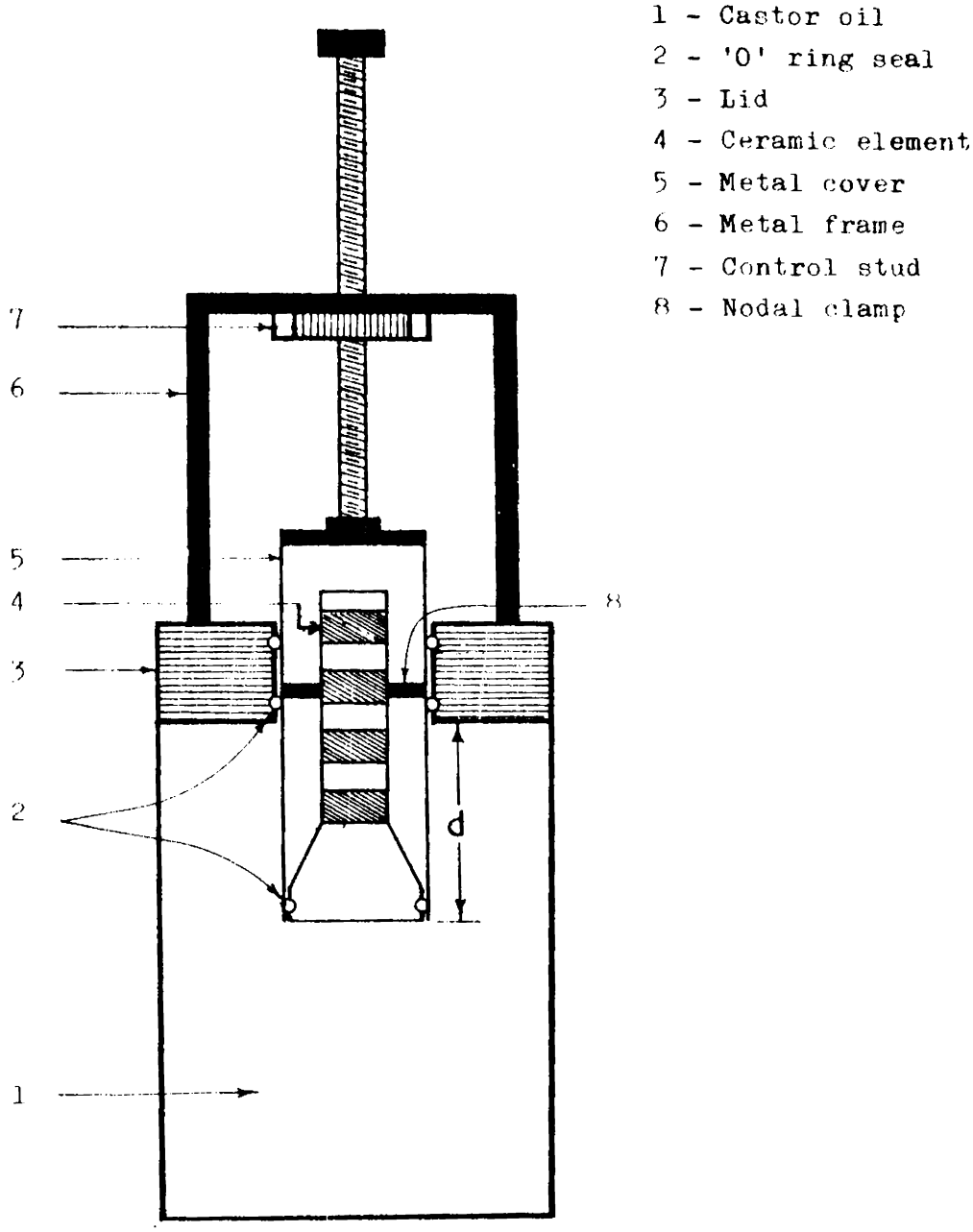

Fig.6.1 : Set-up of the projector assembly, used to investigate the effect of finite medium

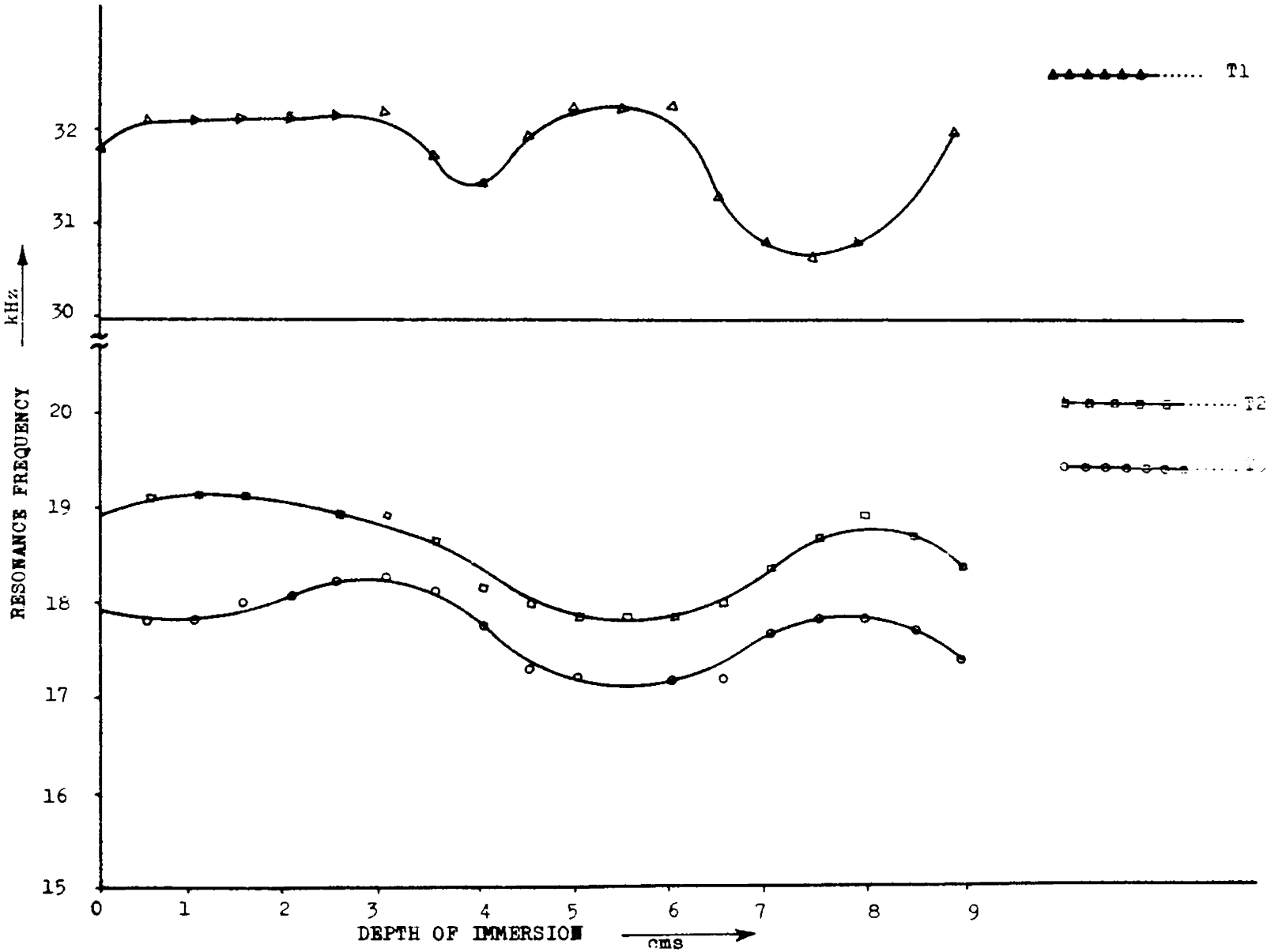

Fig.6.2 : Variation of resonance frequency of ceramic transducer elements with depth of immersion of the radiating face, in a finite medium

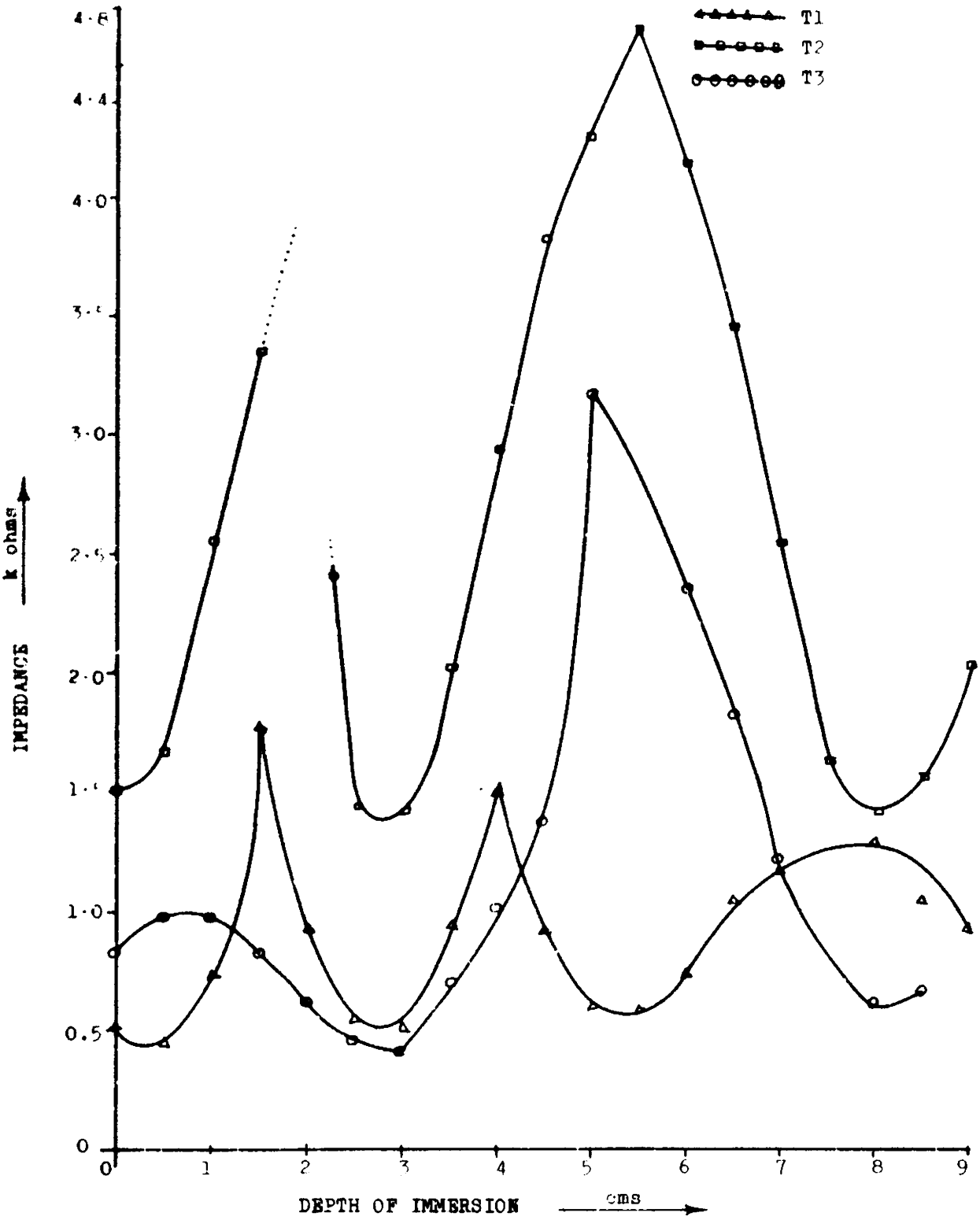

Fig.6.3: Variation of impedance at resonance of ceramic transducer elements with depth of immersion of the radiating face

change in depth of immersion of the radiating face, for three types of ceramic transducers. From these figures, it can be observed that the resonance frequency and impedance at resonance are affected by the depth of immersion and that the variation tends to be periodic. Dimensions and resonance frequencies of these three types of transducer elements are listed in table 6.1.

For various transducers, dimensions of the container and the quantity of castor oil in it were also varied and it was found that the nature of variation also differed slightly. The diameter of the container and the height of the castor oil column, for the most favourable results for a transducer resonant around 20 kHz were found to be 9.5 cms and 10.5 cms, respectively. The resonance frequencies of T2 and T3 are around 18 kHz, while that of T1 is around 32 kHz. The departure of the resonance frequencies of individual elements influence the variation to a great extent, as is clear from Fig.6.2 and Fig.6.3. But, if the dimensions of the container and the quantity of fluid in it are changed, variations similar to that of T2 and T3 will be obtained for T1 also.

The assembly of the transducer element immersed in the container of critical dimensions, was in turn immersed in the acoustic test tank. As was expected, a

Table 6.1

Dimensions and resonance frequencies of various transducers used for investigating finite medium effects.

Particulars of Transducers

Transducer Model	Resonance frequency when the transducer radiates into infinite medium (in kHz)	Cross section of the element	Dimensions of the element	Length of the element	No. of elements in the transducer	Cross section of the radiating face	Dimensions of the radiating face
T1	32	Square	16mm x 16mm	2.5mm	4	Square	27.5mm x 27.5mm
T2	18.5	Circular	22.5mm dia	8mm	4	Square	38.5mm x 38.5mm
T3	18.0	Circular	22mm dia	8.5mm	4	Circular	40mm dia

mere change in depth of immersion of the assembly, as a whole, produced no tangible effect.

6.3 Explanation

The compliance of the transducer C_m is given by [1b]

$$C_m = \frac{s' \, l}{A} \tag{6.1}$$

where

s' = elastic constant of the material of the transducer, measured in m^2/N

l = thickness of the material

A = area of the radiating face

Also, the analysis given in appendix V reveals the cause of variations in equivalent mass M, mechanical resistance R_m and compliance C_m. Variations in C_m cause corresponding variations in s'.

The resonance frequency of the transducer element is [1b]

$$f_r = \frac{\omega_r}{2\pi} \tag{6.2}$$

where the angular resonance frequency ω_r is given by

$$\omega_r = \frac{1}{\sqrt{(M C_m)}} \tag{6.3}$$

The variations in M and C_m clearly explain the observed variations in resonance frequency and impedance at resonance.

6.4 Physical Interpretation of the Variation

Consider a transducer element immersed at a certain depth. When the depth of immersion is varied, the transducer face encounters a different state of the reflected wave, and the resultant pressure at the transducer face varies which in turn varies C_m and hence s'. Also, the transducer experiences different magnitudes of frictional force and a change in its effective mass, due to these pressure variations. The variations in frictional force will cause corresponding variations in its effective resistance. Hence C_m, M and R_m vary under the influence of the reflected signal. The variations of C_m, R_m, M and f_r should be periodic. Observed slight deviations from the periodic variations of impedance at resonance and the resonance frequency are explained as due to the reflections from the walls of the container.

Thus it can be concluded that the resonance frequency and impedance at resonance exhibited by the ceramic transducer element vary with change in depth of immersion of its radiating face in a finite medium.

To a first observation, it appears that the standing wave formation will considerably reduce the radiated pressure level. But, contrary to this prediction, experimental measurements yielded acoustic pressure

levels which are slightly greater, at certain depths of immersion, than the level with direct water-loading in an infinite medium. The measured values of acoustic pressure levels are given in 6.5.2.

6.5 Applications in Array Synthesis

6.5.1 Tuning of Transducer Elements in a Transducer Array [41]

The variation of resonance frequency with depth of immersion of the radiating face of a ceramic transducer element can be used to overcome the problem of small changes in the resonance frequencies of different identical ceramic transducers used in a transducer array. This can be realised by immersing the transducer elements in suitable containers of fluid, whose depths of immersion can be individually controlled. By making fine adjustments to the depths of immersion of the radiating face, the resonance frequencies of all the transducer elements can be equalised. This gives a method to tune the resonance frequencies of all the transducer elements used in the array, permitting their excitation at the common resonance frequency, to increase the efficiency.

The arrangement of transducer elements in a two element transducer array is shown in Fig.6.4. Here the

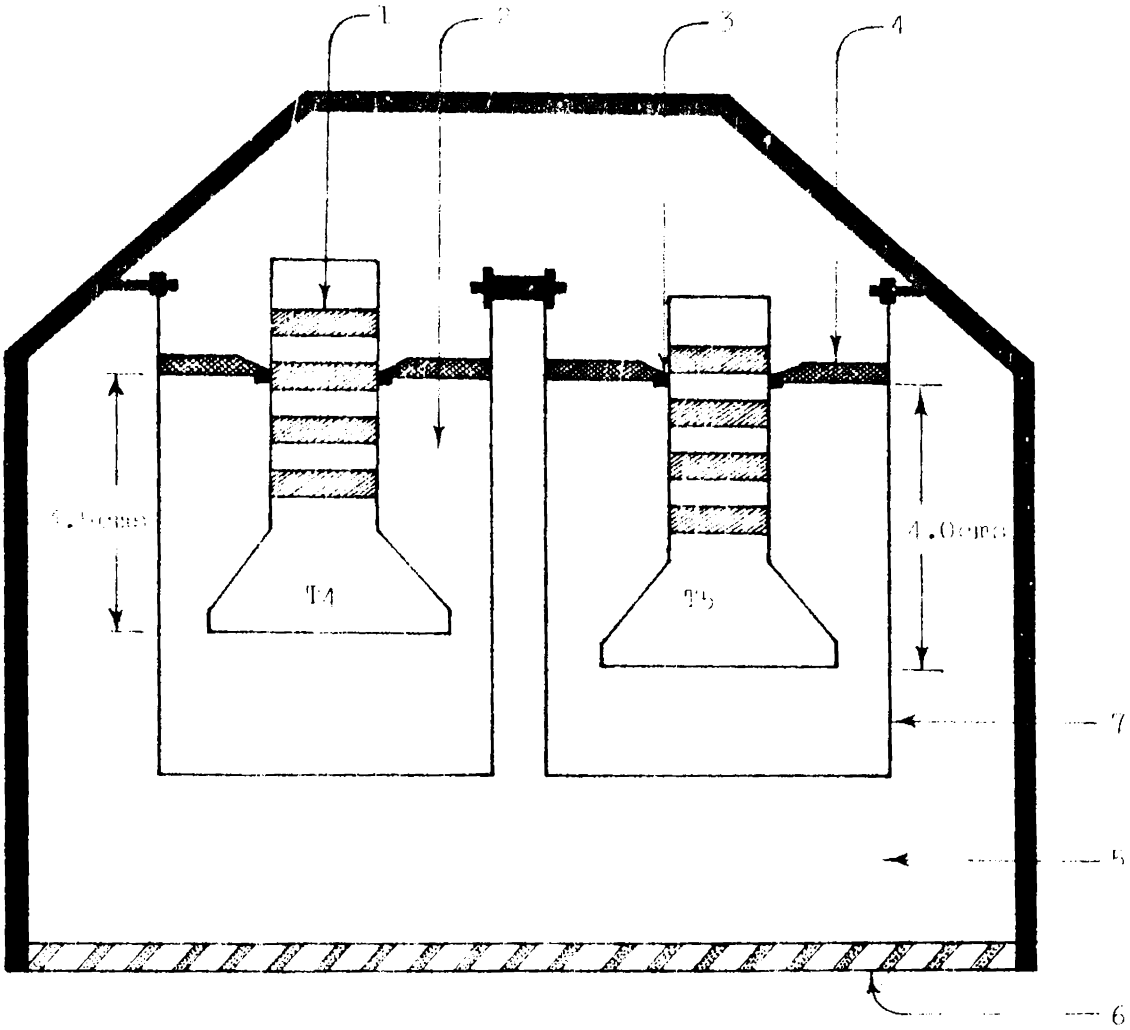

1 - Ceramic Element
2 - Rubber ring
3 - Seal
4 - Cover
5 - Water
6 - Acoustically transparent window
7 - Container

Fig. 4.4 : Arrangement of transducer elements in two element transtuner

transducer elements are immersed in castor oil contained in a cylindrical semi-rigid container of diameter 9.5 cms with a castor oil column of height 10.5 cms. The assembly of the transducer elements immersed at different depths is placed in another container of water with an acoustically transparent window.

The photographs shown in Fig.6.5(i) and Fig. 6.5(ii) are the external view of the two element ceramic transducer array incorporating the tuning facility - 'The Transtuner' - and the individual element assembly enclosed in the semi-rigid container.

In the 2-element 'transtuner assembly', two identical PZT transducer elements T4 and T5, having resonance frequencies 17.9 kHz and 18.9 kHz, respectively at zero depth were used. Table 6.2 shows the resonance frequency variation with depth of immersion of the radiating face in castor oil for the two transducers. The depths of immersion at which the transducers must be operated were so chosen that the transducers individually radiate maximum power at a common resonance frequency.

Each transducer had a square radiating face of dimensions 38.5 mm x 38.5 mm and was composed of 4 ceramic elements, each circular of diameter 22.5 mm and thickness 8 mm.

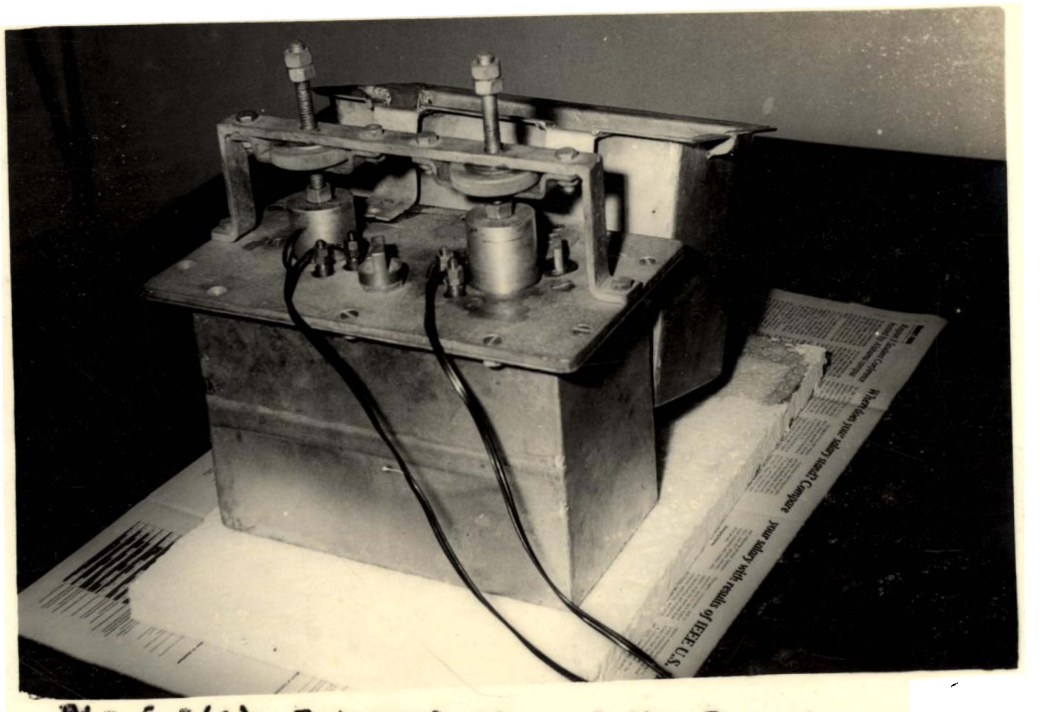

Fig.6.5(i): External view of the Transtuner

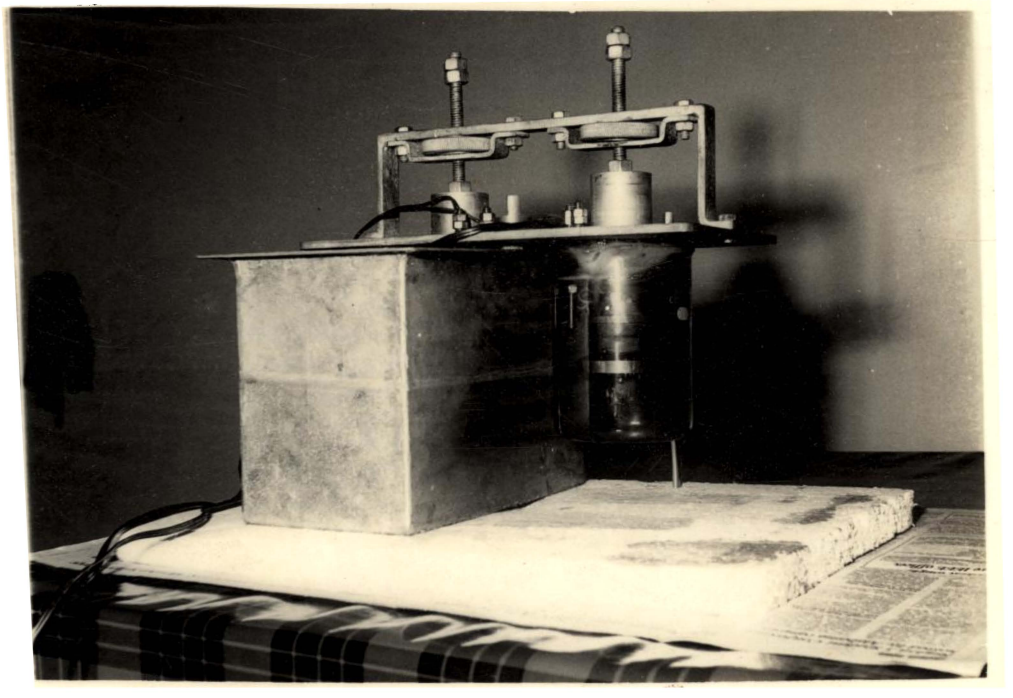

Fig.6.5(ii): Element assembly used in the Transtuner

Table 6.2

Variation of resonance frequencies of the ceramic transducer elements T4 & T5, used in the Transtuner, with depth of immersion of their radiating faces

Depth of immersion of radiating face (cm)	0	0.5	1.0	1.5	2.0	2.5	3.0	3.5	4.0	4.5	5.0	5.5	6.0	6.5	7.0	7.5	8.0	8.5	9.0	9.5	10.0	10.5
Resonance frequency of T4 (Hz)	17985	17814	17815	18001	18085	18214	18221	18092	17747	17289	17200	17175	17150	17255	17295	17525	17675	17652	17508	17270	17262	17258
Resonance frequency of T5 (Hz)	18925	19105	19120	19115	19000	18910	18908	18612	18111	17951	17795	17794	17957	18175	18465	18665	18672	18524	18414	18312	18413	18575

When T5 is at a depth of 4.0 cm and T4 at 2.0 cms and 3.5 cms, their resonance frequencies are nearly equal as is clear from table 6.2. Other depths of immersion at which resonance frequencies will be equal are also possible, provided the power radiated is maximum.

6.5.2 Maximum Achievable Efficiency of a Ceramic Transducer Element

Experimental set-up and Measurements

Investigations on the efficiency variation with depth of immersion of the radiating face of a ceramic transducer element were carried out with the projector assembly shown in Fig.6.1 and the experimental set-up of Fig.6.6. The projector assembly was immersed in the acoustic test tank. The measurement consists of determining the electrical equivalent resistance of the transducer at resonance, the radiated pressure level and the efficiency of radiation of the transducer element used in the projector assembly at every 5 mm depth of immersion of its radiating face in castor oil. A Brüel and Kjaer model 8100 standard hydrophone kept at 1 metre from the assembly, along its axis was used to measure the acoustic pressure level. The efficiency of radiation of the transducer element was evaluated with the help of the admittance diagram [1c],[5], shown in Fig.6.7, obtained with air and castor oil loading

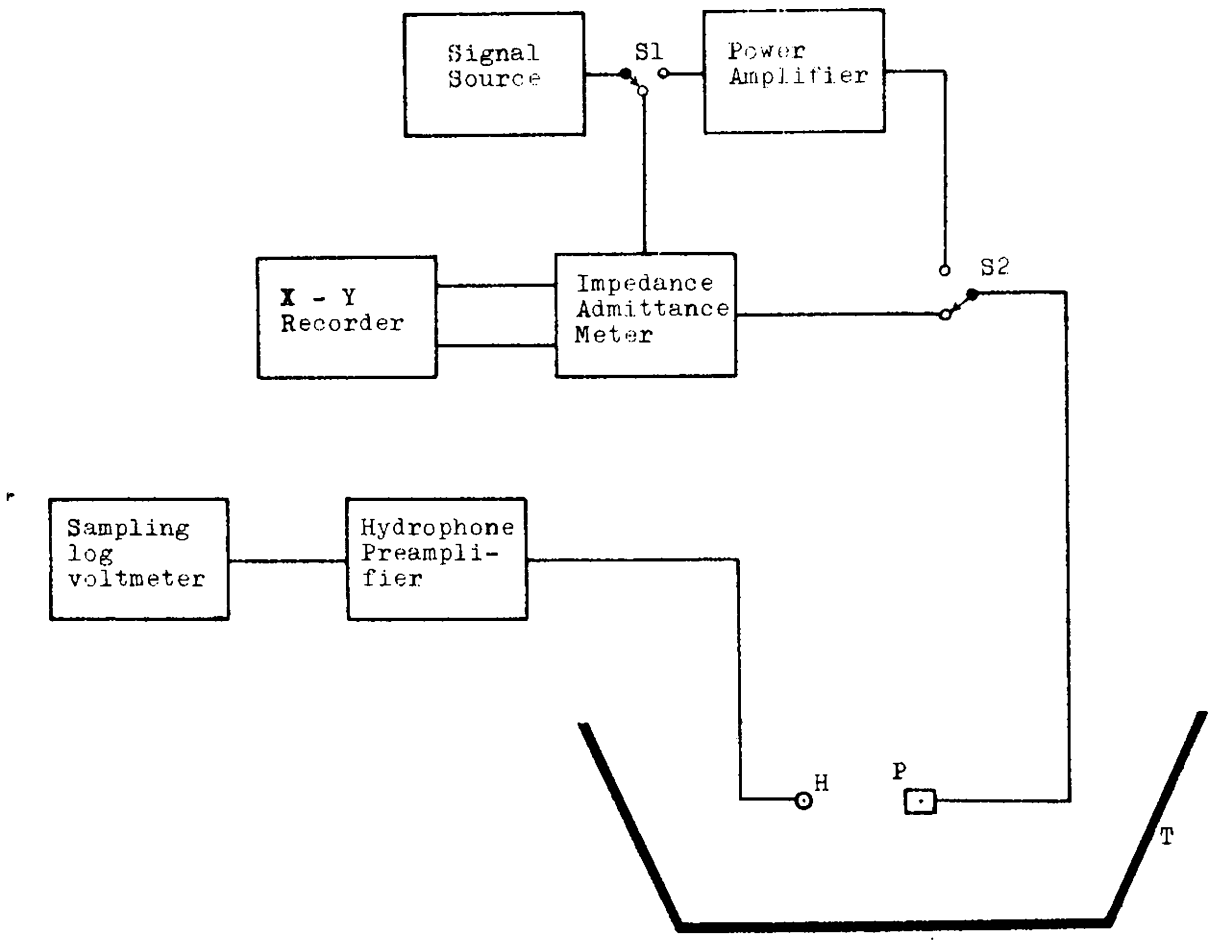

Fig.6.6 : Experimental set-up for investigating the effect of depth of immersion on the efficiency of radiation of a ceramic transducer element

H : B and K 8100 Standard hydrophone

P : Projector Assembly of Fig.6.1

T : Test tank

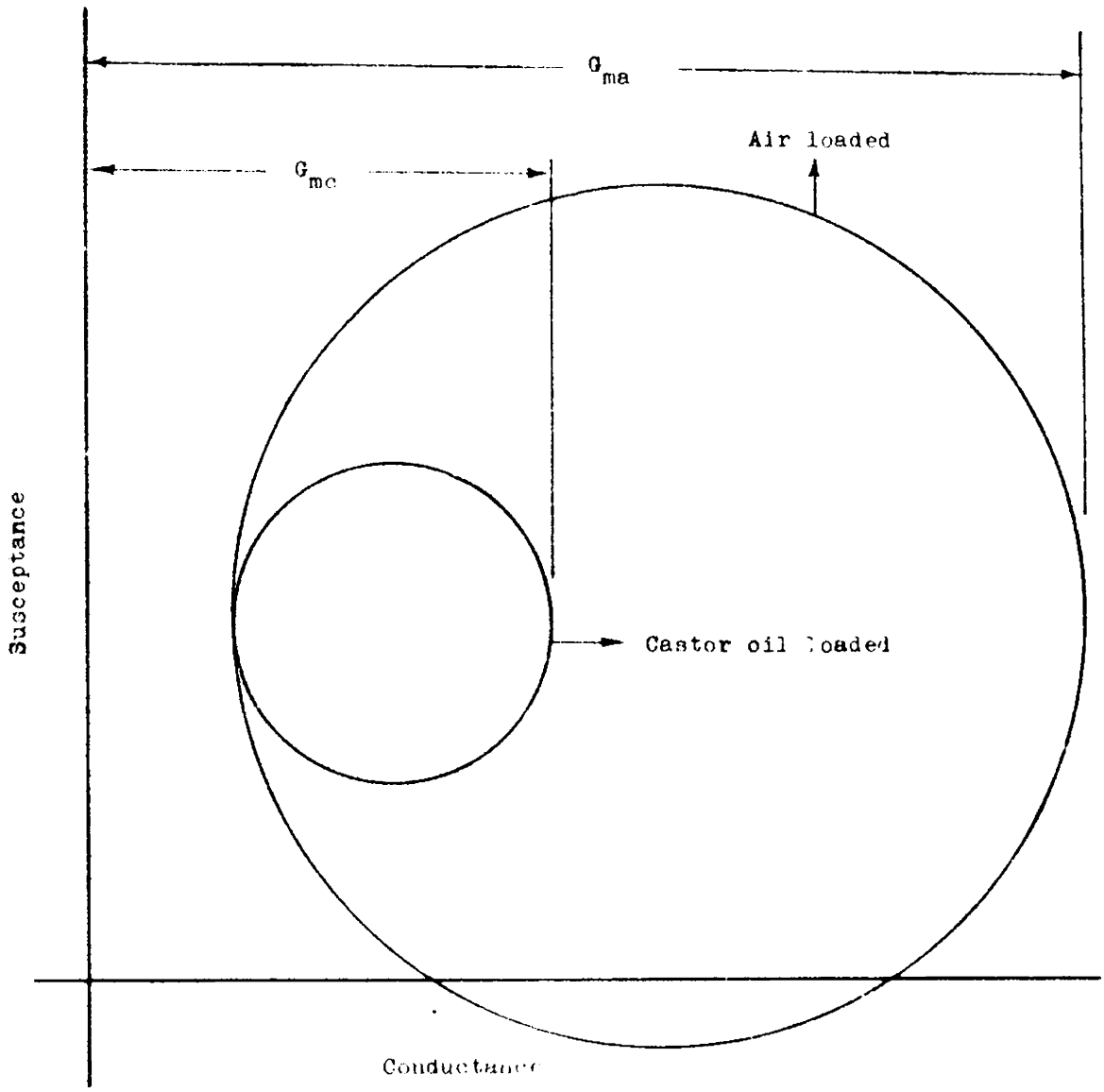

Fig.6.7 : Admittance diagram of ceramic transducer elements with air and castor oil loadings

around its resonance frequency, using the expression [5],

$$\eta = \left(\frac{D_a}{D_c}\right) \left[\left(\frac{G_{ma}}{G_{mc}}\right) - 1\right] \qquad (6.4)$$

where

D_a = circle diameter for air loading

D_c = circle diameter for castor oil loading when the projector assembly radiates into the infinite medium.

G_{ma} = maximum conductance in air

G_{mc} = maximum conductance in castor oil.

Automatic plotting of the admittance diagrams were obtained with a calibrated X-Y Recorder, driven by the D.C. output signals of a Dranetz model 100-C Complex Impedance - Admittance Meter, by sweeping the signal source around the transducer resonance.

Experimental Results

Admittance diagrams, electrical equivalent resistance of the transducer at resonance and the acoustic pressure levels were obtained for direct water loading and castor oil loading at various depths of immersion. From these diagrams, the efficiencies of radiation of the transducer when radiating into water, directly and through the assembly at various depths of immersion in castor oil

were evaluated using (6.4). Table 6.3 shows the variation of electrical equivalent resistance of the transducer at resonance, efficiency of radiation and acoustic pressure level, for a constant driving signal, with depth of immersion. At a depth of immersion of 5.0cm in castor oil, the efficiency of radiation is 74.42 % while that for direct water loading is 69.51 % as is clear from the table.

The measured values of the acoustic pressure levels, given in table 6.3 are the results obtained by connecting the power amplifier in the transmitting circuit by changing the positions of the switches S1 and S2.

The acoustic pressure levels shown in table 6.3 reveals that the excess pressure radiated by the assembly, at certain depths of immersion, is more than sufficient to compensate the power loss due to the enclosure.

The observed influence of the depth of immersion on the efficiency of radiation can be explained in terms of the basic acoustic theory.

It is observed from table 6.3 that the maximum efficiencies of radiation occur when the height of the castor oil column, below the radiating face of the transducer, is approximately an integral multiple of $\lambda/2$.

Table 6.3

Variation of equivalent electrical resistance, efficiency of radiation and radiated acoustic pressure levels with depth of immersion of the radiating face of a ceramic transducer element

Depth of immersion of the radiating face (cm)	0	0.5	1.0	1.5	2.0	2.5	3.0	3.5	4.0	4.5	5.0	5.5	6.0	6.5	7.0	7.5	8.0	8.5	9.0	9.5	10.0	10.5
Equivalent electrical resistance (KΩ)	1.25	1.11	1.21	1.67	5.0	3.0	3.33	3.13	2.86	2.63	2.5	2.38	2.63	3.33	4.0	4.35	5.0	4.35	4.0	3.0	3.46	3.5
Efficiency of radiation (%)	62.84	60.33	65.91	71.43	71.01	71.01	72.72	73.39	73.73	74.35	74.43	74.39	74.31	73.57	70.55	64.82	62.53	65.81	66.70	64.83	62.63	61.23
Acoustic pressure level (Pa)	5.34	5.27	5.56	5.85	5.77	5.81	5.85	5.88	5.90	5.92	5.92	5.92	5.92	5.85	5.72	5.52	5.34	5.59	5.63	5.52	5.48	5.35

Measurements with direct water loading :

Equivalent electrical resistance = 3KΩ
Efficiency of radiation = 69.51%
Acoustic pressure level = 5.774 Pa

This dependence can be explained as follows. Consider an instant at which the transducer had compressed the fluid medium, in contact with its radiating face. During the time this compression arrives at the radiating face, after reflecting from the bottom of the container, the transducer will be compressing the fluid if and only if the height of the castor oil column is an integral multiple of $\lambda/2$. Similar arguments holds for the rarefaction also. This case corresponds to the maximum radiated acoustic pressure and hence the maximum efficiency of radiation.

Thus, it follows that the observed variation in efficiency of radiation is not merely due to the variations in coupling coefficient.

Though, these variations are presented for a single transducer element, the same can be extended to a sonar array.

6.5.3 Selection of Q-factor

Any desired Q-factor, within certain limits, can be introduced by this effect.

In most of the underwater applications involving the transmission of acoustic pulses of short duration, transducers of wide bandwidth are required [1c].

This shows that the Q-factor of the transducer element plays an important role in underwater propagation. The mechanical Q-factor Q_m and the electrical Q-factor Q_e of transducers are defined as [1c],

$$Q_m = \frac{\omega_r M}{R_m} \tag{6.5}$$

$$Q_e = \omega_r C_o R \tag{6.6}$$

where

$$R_m = \rho c A, \tag{6.7}$$

ρ being the density of the fluid medium and

c the velocity of propagation.

$$\omega_r = 2\pi f_r, \tag{6.8}$$

the angular resonance frequency.

$$R = \frac{R_m}{\alpha^2}, \tag{6.9}$$

α being the transformation ratio measured in C/m, given by

$$\alpha = \frac{Ae'}{l} \quad \text{and} \tag{6.10}$$

e' being the piezoelectric stress coefficient, measured in N/Vm

Also, Q_m and Q_e are related as,

$$Q_e = \frac{\pi^2}{2Q_m k_c^2} \qquad (6.11)$$

for symmetrically loaded element

where

k_c = the coupling coefficient.

Thus, Q_m can be decreased by loading, resulting in a high Q_e. Any Q-factor, depending on the loading, can be introduced by suitably adjusting the depth of immersion of its radiating face in the fluid taken in the container of critical dimensions.

6.5.4 Impedance-Matching in Sonar Arrays

Matching the load of the transducer to that of the generator imposes a serious problem to a sonar engineer. This problem can be solved, to some extent, by the effect of impedance variation with depth of immersion. It is to be noted that trimming in impedance at resonance is fairly easy in the proposed method.

The dimensions of the container given in section 6.2, for better results, are larger when compared with the wavelength of acoustic radiation. Experimental results revealed that, even small containers are capable of producing almost similar variations, with depth of immersion.

In order to make the system of transducer array synthesised on this basis light, the outer metallic enclosure can be replaced by a metallic frame, on which is fixed an acoustically transparent window. Also, it is recommended to fill the whole of the container with castor oil, in order to make sure that the performance characteristics remain unaltered, in case if the array system is inverted or tilted.

6.6 Applications in Nonlinearity Study

With a given transducer, the operation at high efficiency is restricted to a narrow band around its resonance frequency. Therefore, any experimental verification of a model for the medium is possible only in a limited range of frequencies. Various transducers have to be used for studying the characteristics at different frequencies.

By means of the proposed technique of enclosing a transducer in a suitable container of fluid and varying its depth of immersion, a very wide range of resonance frequencies can be realised for the same transducer. This is of great help in comprehensive characterisation of the medium.

Also, two identical transducer elements immersed to different depths resonate at different frequencies

and consequently the parametric effects can be simulated more effectively.

6.7 Conclusion

It is experimentally shown that the depth of immersion of the radiating face of a ceramic transducer element has a remarkable influence on its resonance frequency and impedance at resonance. The variation is almost periodic. The experimental results presented in sections 6.5.1, 6.5.2, 6.5.3 and 6.5.4 show the usefulness of this effect towards tuning of transducer elements in a ceramic transducer array, the maximum efficiency of radiation setting of individual elements to achieve the maximum array gain, Q-factor selection and trimming in impedance. Application towards nonlinearity study is also discussed.

CHAPTER VII

C O N C L U S I O N

7.1 Introduction

An assessment of the work presented in preceeding chapters along with the highlights and scope for future developments is made here. It is expected that the results derived in the previous chapters will be of great use in the designing of underwater transducer arrays, which is the brain of an underwater sensor.

7.2 Brief Survey of the Work Towards the Scope for Future Developments.

Different LPA formats, which conform to Carson's suggestion were discussed in chapter II. Of the various results, the most significant beam patterns were shown in Fig.2.2 (i) and Fig.2.2(ii) and important operational features of the others were briefly represented in different tables. Any array format can be realised, by switching the required elements of a CPPA, with the help of the programmable switching system, described in chapter III. Programs for

different array formats can be developed and appropriate programs can be called from the read memory of the system, depending on the purpose.

Also, considerably better side lobe suppressions, than those discussed in chapter II, can be achieved by selectively switching some of the elements of the CPPA, as judged by their orientations. Also, all the drawbacks of the LPA format can be rectified by suitably implementing the switching system in conjunction with a CPPA. Thus higher array gain, lobe switching and amplitude shading, by the 'SAAT' technique, are achieved through suitable programs, without the necessity of additional hardware. The microprocessor based switching system is designed and fabricated with the intention to reduce the human effort in the technology of array synthesis.

Contrary to single frequency operation, the beam pattern of the difference frequency signal is not related to the aperture area. However, the radiating aperture has slight influence on the beam pattern through the so called 'aperture factor'. Also, in the proposed application of the LPA format towards nonlinearity study, the central and the alternating elements are excited by one of the primary frequencies, while the rest of the elements by the second, thus enhancing the chance of interaction between the

primary radiations and reducing the length of the interaction column.

It is pointed out, in chapter VI, that the depth of immersion of the radiating face of a ceramic transducer element in a finite medium influences the resonance frequency, impedance at resonance, the Q-factor, the efficiency of radiation and the related parameters. Applications of this phenomenon towards array synthesis and nonlinearity study were described. However, it appears that the application towards

(i) Tuning of transducer elements in a transducer array and

(ii) Operation at maximum efficiency by selecting the optimum depth of immersion of each element

are difficult, if employed simultaneously. But it is expected that by varying the quantity of fluid in the container and the container dimensions, it may be possible to achieve the maximum efficiency of the array by tuning all the elements to the common resonance frequency and also by maximum efficiency setting of each element. No technique, other than this 'trial and error' is possible because too little theory is available for the explanation of this variation. If the maximum acoustic power conversion of the array is achieved by employing both these techniques together, the source level will be greater than, that

when they are employed separately. If this condition is attained, then modifications to the radiation pattern can be achieved with the help of the switching system. The theoretical analysis of the beam pattern in this case will be more complicated, as the radiating faces of all the elements are not in the same plane.

7.3 Highlights

The highlights of this thesis are as follows:

1. It is for the first time, in the field of 'Underwater Acoustics', that an LPA format to reduce the 'interaction effects' is proposed.
2. A microprocessor based switching system to synthesise any desired array format, including an LPA out of a CPPA has been suggested. An example for switching few elements of a CPPA has been appended.
3. Applications of the switching system towards amplitude shading by the 'SAAT' technique, have been proposed. 'Binomial Shading' and 'Dolph-Chebyshev Shading' have been illustrated as the specific examples for the 'SAAT' operation. Programs have also been included in the appendix.

4. A programmable CPPA format can be used for achieving higher array gain, in case if the measurement is taken under conditions of low signal-to-noise ratio. Switching the main lobe to any direction depending on the region to be insonified is also possible.

5. Application of the LPA format in the generation of narrow beam low frequency sound waves, through nonlinear interactions has been suggested. Advantages of the nonlinearly generated low frequency signal will offset the disadvantage caused by the inefficient power conversion mechanism.

6. The problem of slight changes in the resonance frequencies of various identical ceramic transducer elements used in an array can be easily solved by enclosing them in a semi-rigid container filled with castor oil and adjusting the depth of immersion. Earlier methods employed for tuning the elements, were too expensive.

7. Finite medium effects can be advantageously exploited to enhance the array gain, by setting each element at that depth of immersion to get the maximum efficiency of radiation.

8. The problem of impedance-matching in sonar arrays can be solved, to some extent, by the finite medium

effects, thus reducing the standing wave formation between the projector array and the generator.

9. Any model for the medium can be studied over a a wide range of frequencies by enclosing a narrow-band transducer element in a suitable container of fluid.

10. Parametric effects, at the maximum efficiency, can be simulated over a wide range of frequencies, starting from the lowest using two identical ceramic transducer elements.

11. The work presented in this thesis has to its credit two publications [41],[42].

The switching system will be very useful in switching the required staves of the cylindrical type transducer array reported in [4c] and the huge 30-ton AN/SQS-26 [10], the largest transducer array in the world, manufactured by Edo Western Corporation.

7.4 Present Status of the Work

Though a group of U.S. scientists, organized by the National Defence Research Committee, were the pioneers in the field of 'Underwater Acoustics', work in this field is now being extended to the Defence and R and D organization of almost all the countries. Also, the military

aids, which the field provided during its period of origin, are presently being spread to the nonmilitary fields like depth sounding, fish finding, position marking, divers' aids etc..

Majority of the results that were recorded by the NDRC as confidential and labelled as RED BOOKS, even now remain unpublished. Hence, it is not possible to get a clear picture of the present status of the work, due to its military importance.

A P P E N D I C E S

APPENDIX I

APPLICATIONS OF UNDERWATER SOUND

Table I.1: Military applications of underwater sound

Sl.No.	Function	Description
1.	Acoustic mines	A sensor of acoustic radiation, which explodes when the acoustic level in its pass-band reaches a critical value.
2.	Minesweeping operation	Here acoustic mines are purposely exploded by the sound of a powerful source.
3.	Submarine detection	
4.	Homing Torpedoes	Make use of moderately high frequencies.
5.	Underwater Telephone	For communicating between a ship and a submarine or between two submarines.
6.	Sonobouys	Small sonar sets used for underwater listening and echo-ranging.

Table I.2: Nonmilitary applications of underwater sound

Sl.No.	Function	Description
1.	Bathymetry or Depth Sounding	Operating mostly in the frequency band 10 kHz to 100 kHz.
2.	Sub-bottom Profiling or Seismic Profiling	High power sources at low frequencies are used.
3.	Side Scan Sonar	Mapping the sea bed at right angles to ship's track.
4.	Doppler Navigation	Here pairs of transducers are used for determining speed over the bottom from the doppler shift of the bottom returns.
5.	Fish Finding	Locating schools of fish both for research and industry.
6.	Position marking Transponders	Transmit sound wave when suitably interrogated.
7.	Communication and Telemetry	Transmitting information.
8.	Acoustic Flow meter	Measuring speeds of currents.
9.	Acoustic wave height meter	Works as an inverted echo-sounder.
10.	Velocimeter	Measuring velocity of sound.
11.	Bathy thermograph	For measuring temperature.
12.	Divers' Aids	Small hand-held sonar sets for underwater object location by divers.

APPENDIX II

DETAILS OF OUTPUT PORTS

The output ports named as Port 06, Port 07, Port 08, ... Port 26 in hex code are accessible in the switching system. Decoded outputs are available on the board for providing an additional 218 output ports.

It is to be noted that each port of this system can control 8 transducer elements. Thus the 32 ports presently accessible will control 256 elements. The controlling of 32 elements through 4 output ports, namely Port 06, Port 07, Port 08 and Port 09 is illustrated in the latching unit of Fig.A.II.1.

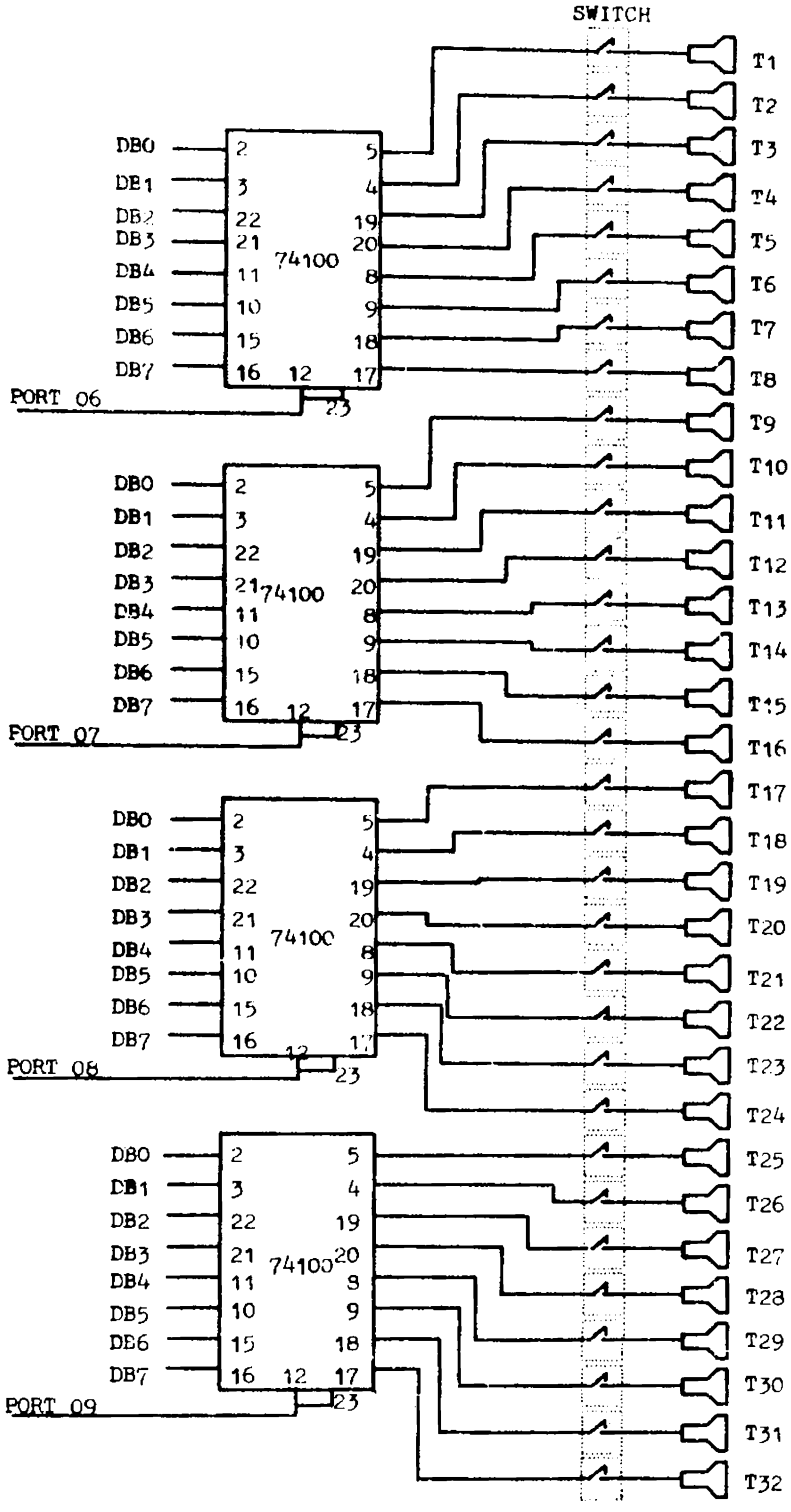

Fig.A.II.1: LATCHING UNIT OF THE SWITCHING SYSTEM

APPENDIX III

PROGRAM FOR THE SELECTIVE SWITCHING

The flow chart and the program for switching the elements T1, T2, T7, T8, T9, T11, T14, T16, T19, T20, T23, T25, T27, T29 and T31, which are connected to various bits of Port 06, Port 07, Port 08 and Port 09 as shown in Fig.A.II.1, is given below.

Flow Chart for Selective Switching

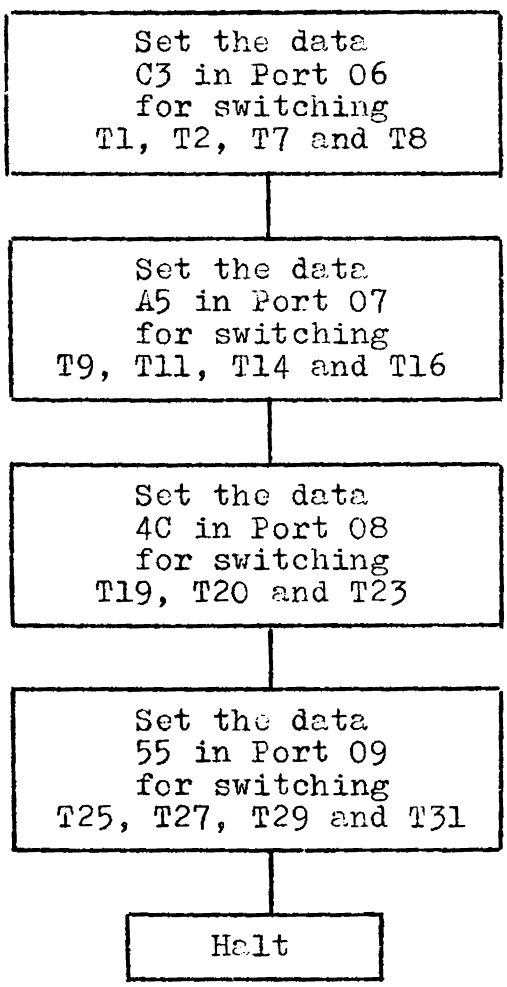

Program for selective switching

Address		Op Code	Mnemonic	Comments
HI	LO			
04	00	3E	MVI, A	Set the data C3
04	01	C3	C3	in Port 06
04	02	D3	OUT	
04	03	06	PORT 06	
04	04	3E	MVI,A	Set the data A5
04	05	A5	A5	in Port 07
04	06	D3	OUT	
04	07	07	PORT 07	
04	08	3E	MVI, A	Set the data 4C
04	09	4C	4C	in Port 08
04	0A	D3	OUT	
04	0B	08	PORT 08	
04	0C	3E	MVI, A	Set the data 55
04	0D	55	55	in Port 09
04	0E	D3	OUT	
04	0F	09	PORT 09	
04	10	76	HLT	Halt

APPENDIX IV

PROGRAMS FOR THE SPECIFIC EXAMPLES OF SAAT OPERATION

Let the transducer elements T1, T2, T11, T12, T21 and T22, out of the CPPA which are connected to the switching system as shown in Fig. A.II.1, form a 6-element linear array. The output switching time durations for the different elements, the flow charts and the programs for Binomial shading, Dolph-Chebyshev Shading and Continuous Distribution Shading, by the SAAT technique, are given in sections A.IV.1, A.IV.2 and A.IV.3, respectively.

A.IV.1 Binomial Shading

The output switching time durations for different elements in a Binomial array is illustrated in Fig.A.IV.1. The Flow Chart and the program for the output switching time control is given below.

Flow Chart

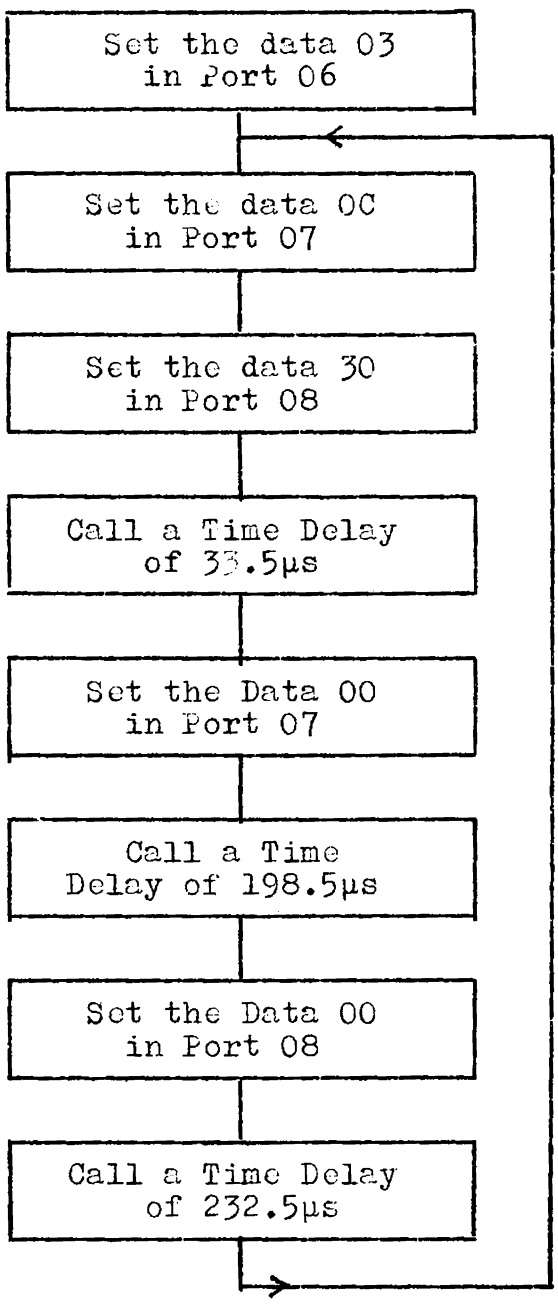

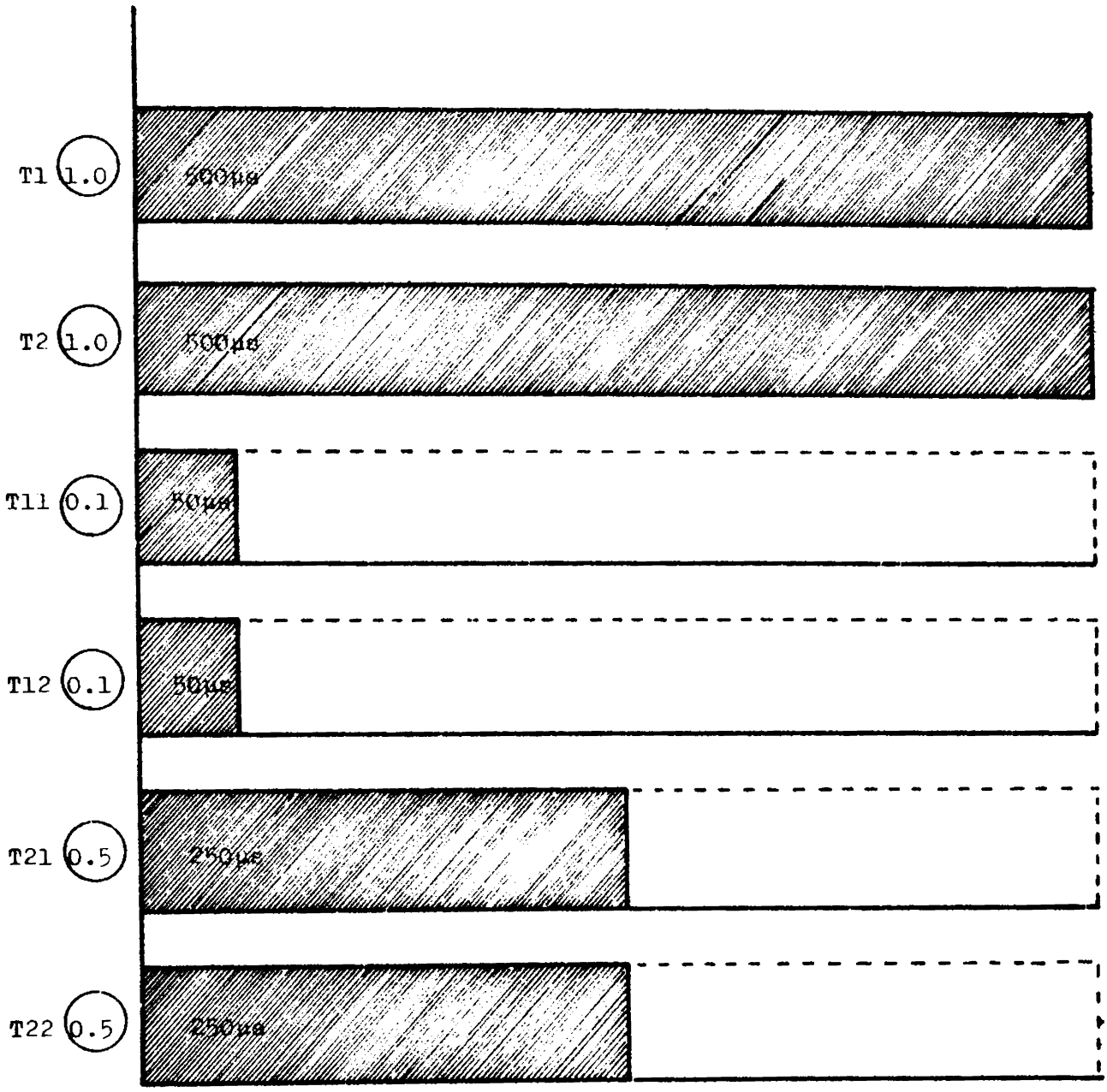

Fig.A.IV.1 : Output switching time durations for different elements of a 6-element linear array for the Binomial Shading
T1 and T2 are connected to bits 1 and 2 of Port 06
T11 and T12 are connected to bits 3 and 4 of Port 07
T21 and T22 are connected to bits 5 and 6 of Port 08

Program for the Output Switching for a Binomial Array

Address		Op Code	Mnemonic	Comments
HI	LO			
04	00	3E	MVI, A	Set the Data
04	01	03	03	03 in Port 06
04	02	D3	OUT	
04	03	06	PORT 06	
				Point x
04	04	3E	MVI, A	Set the Data
04	05	0C	0C	0C in Port 07
04	06	D3	OUT	
04	07	07	PORT 07	
04	08	3E	MVI, A	Set the Data
04	09	30	30	30 in Port 08
04	0A	D3	OUT	
04	0B	08	PORT 08	
04	0C	06	MVI, B	Call a Time
04	0D	04	04	Delay of 33.5μs
04	0E	05	DCR, B	
04	0F	C2	JNZ	
04	10	0E	0E	
04	11	04	04	
04	12	3E	MVI, A	Set the Data
04	13	00	00	00 in Port 07
04	14	D3	OUT	
04	15	07	PORT 07	

Address		Op Code	Mnemonic	Comments
HI	LO			
04	16	06	MVI, B	Call a Time
04	17	1A	1A	Delay of 198.5µs
04	18	05	DCR, B	
04	19	C2	JNZ	
04	1A	18	18	
04	1B	04	04	
04	1C	D3	OUT	Set the Data
04	1D	08	PORT 08	00 in Port 08
04	1E	06	MVI, B	Call a Time
04	1F	1E	1E	Delay of 232.5µs
04	20	05	DCR, B	
04	21	C2	JNZ	
04	22	20	20	
04	23	04	04	
04	24	00	NOP	
04	25	00	NOP	
04	26	C3	JMP	Go to POINT 'x'
04	27	04	04	
04	28	04	04	

A.IV.2 Dolph-Chebyshev Shading

The switching time durations for generating a Dolph-Chebyshev array is shown in Fig.A.IV.2. The Flow Chart and the program for this type of Array is given below.

Flow Chart

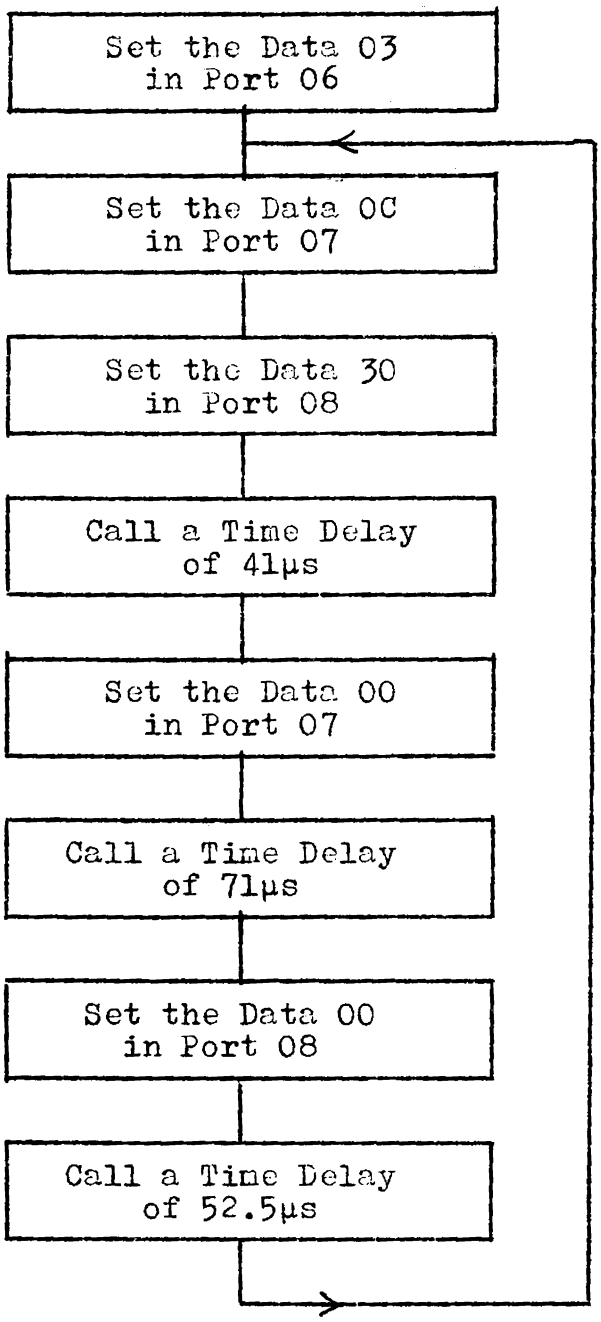

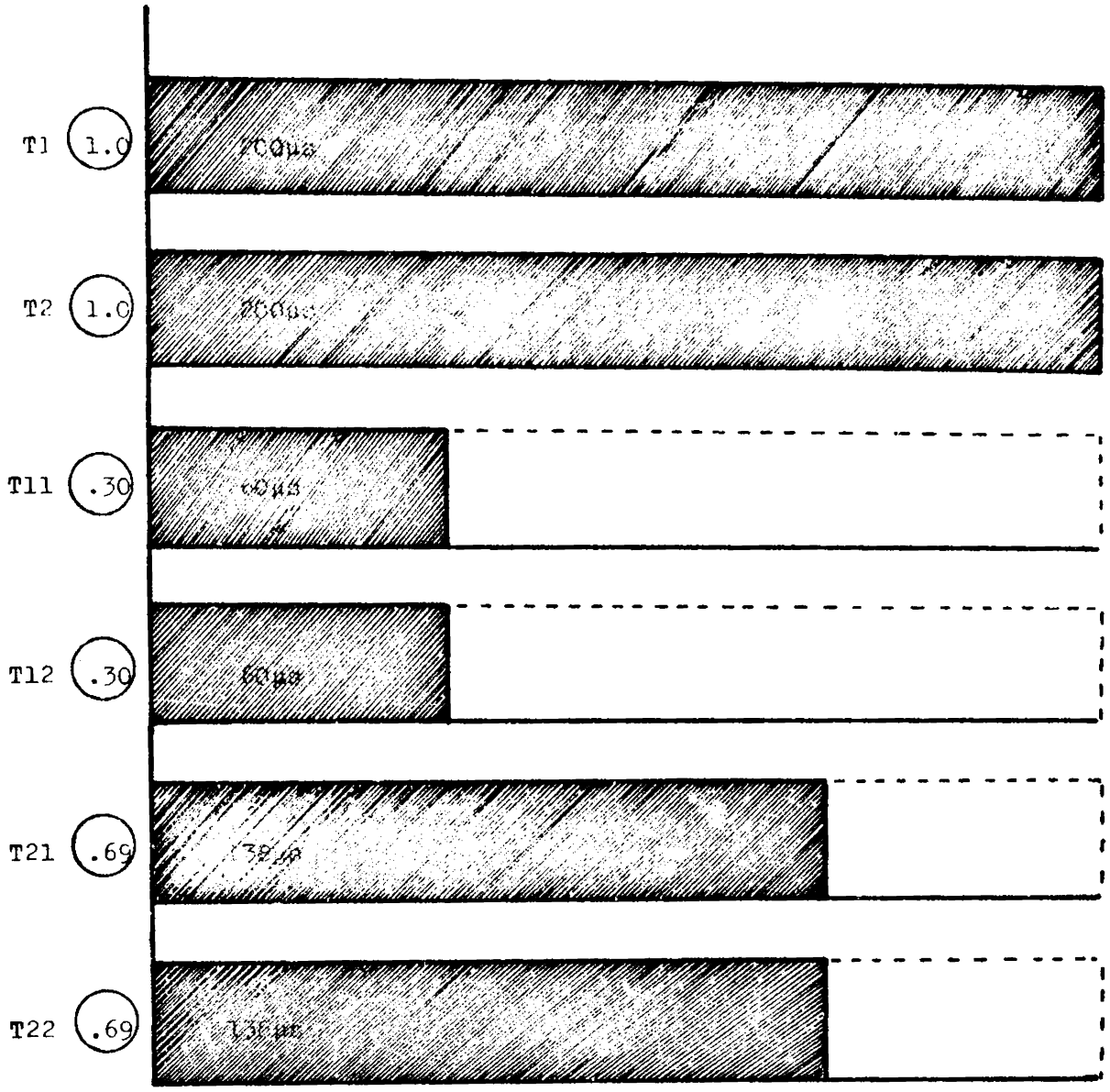

Fig.A.IV. 2 : Output switching time durations for various elements of a 6-element linear array for the Dolph-Chebyshev Shading
T1 and T2 are connected to bits 1 and 2 of Port 06
T11 and T12 are connected to bits 3 and 4 of Port 07
T21 and T22 are connected to bits 5 and 6 of Port 08

Program for the Output Switching for a Dolph-Chebyshev Array

Address HI	Address LO	Op Code	Mnemonic	Comments
04	00	3E	MVI, A	Set the Data 03
04	01	03	03	in Port 06
04	02	D3	OUT	
04	03	06	PORT 06	
04	04	3E	MVI, A	POINT 'x'
04	05	0C	0C	Set the Data 0C in Port 07
04	06	D3	OUT	
04	07	07	PORT 07	
04	08	3E	MVI, A	Set the Data 30
04	09	30	30	in Port 08
04	0A	D3	OUT	
04	0B	08	PORT 08	
04	0C	06	MVI, B	Call a Time Delay
04	0D	05	05	of 41 μs
04	0E	05	DCR, B	
04	0F	C2	JNZ	
04	10	0E	0E	
04	11	04	04	
04	12	3E	MVI, A	Set the Data 00
04	13	00	00	in Port 07
04	14	D3	OUT	
04	15	07	PORT 07	

Address		Op Code	Mnemonic	Comments
HI	LO			
04	16	06	MVI, B	Call a Time Delay of 71μs
04	17	09	09	
04	18	05	DCR, B	
04	19	C2	JNZ	
04	1A	18	18	
04	1B	04	04	
04	1C	D3	OUT	Set the Data 00 in Port 08
04	1D	08	PORT 08	
04	1E	06	MVI, B	Call a Time Delay of 52.5μs
04	1F	06	06	
04	20	05	DCR, B	
04	21	C2	JNZ	
04	22	22	22	
04	23	04	04	
04	24	00	NOP	
04	25	00	NOP	
04	26	C3	JMP	Go to POINT 'x'
04	27	04	04	
04	28	04	04	

A.IV.3 Continuous Distribution Shading

The switching time durations for different elements for continuous distribution shading is shown in Fig. A.IV.3. The flow chart and the program for the output switching time control for this type of array is given below.

Flow Chart

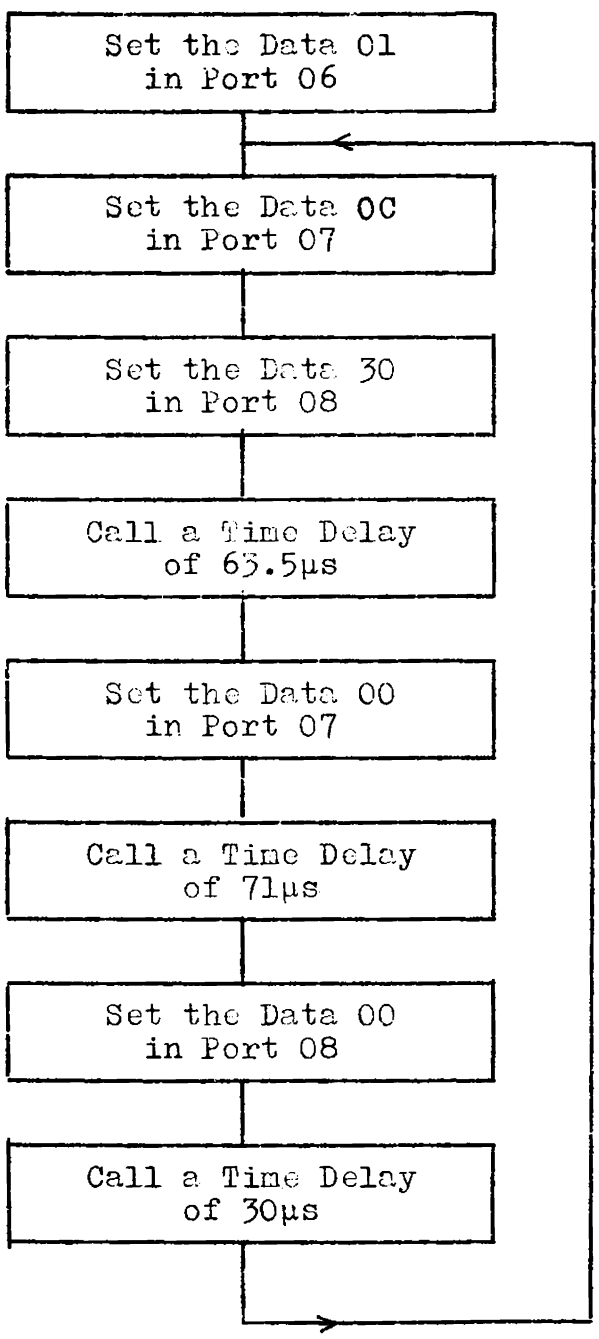

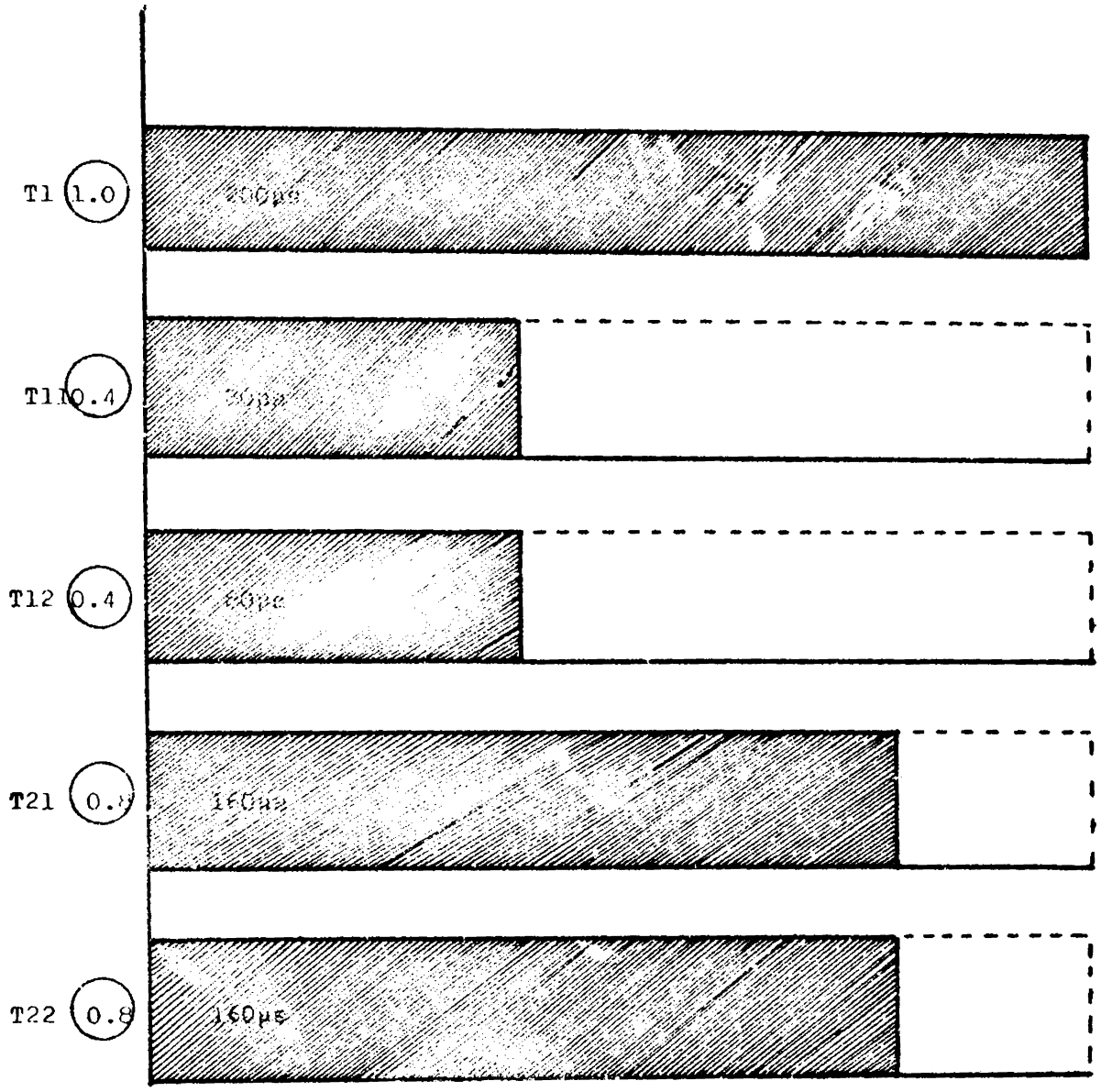

Fig.A.IV. 3: Output switching time durations for various elements of a 5-element linear array for the continuous Distribution Shading

T1 is connected to bit 1 of Port 06
T11 and T12 are connected to bits 3 and 4 of Port 07
T21 and T22 are connected to bits 5 and 6 of Port 08

Program

Address HI	Address LO	Op Code	Mnemonic	Comments
04	00	3E	MVI, A	Set the Data 01 in Port 06
04	01	01	01	
04	02	D3	OUT	
04	03	06	PORT 06	
04	04	3E	MVI, A	POINT 'x' Set the Data 0C in Port 07
04	05	0C	0C	
04	06	D3	OUT	
04	07	07	PORT 07	
04	08	3E	MVI, A	Set the Data 30 in Port 08
04	09	30	30	
04	0A	D3	OUT	
04	0B	08	PORT 08	
04	0C	06	MVI, B	Call a Time Delay of 63.5μs
04	0D	08	08	
04	0E	05	DCR, B	
04	0F	C2	JNZ	
04	10	0E	0E	
04	11	04	04	
04	12	3E	MVI, A	Set the Data 00 in Port 07
04	13	00	00	
04	14	D3	OUT	
04	15	07	PORT 07	

Address HI	Address LO	Op Code	Mnemonic	Comments
04	16	06	MVI, B	Call a Time Delay of 71μs
04	17	09	09	
04	18	05	DCR, B	
04	19	C2	JNZ	
04	1A	18	18	
04	1B	04	04	
04	1C	D3	OUT	Set the Data 00 in Port 08
04	1D	08	PORT 08	
04	1E	06	MVI, B	Call a Time Delay of 30μs
04	1F	03	03	
04	20	05	DCR, B	
04	21	C2	JNZ	
04	22	22	22	
04	23	04	04	
04	24	00	NOP	
04	25	00	NOP	
04	26	C3	JMP	Go to POINT 'x'
04	27	04	04	
04	28	04	04	

APPENDIX V

THEORETICAL ANALYSIS FOR THE EFFECT OF FINITE MEDIUM

The differential equation [1b], governing the motion of the transducer, excited by an external sinusoidal force of angular frequency ω of the form, $F(t) = F \sin \omega t$ is

$$M \frac{du}{dt} + R_m u + \frac{1}{C_m} \int u dt = F \sin \omega t \qquad (V.1)$$

where

M = equivalent mass of the vibrating transducer

R_m = mechanical resistance, measured in kg/s

C_m = compliance and it is the extension produced by unit applied force measured in m/N

u = velocity amplitude of the transducer, measured in m/s

When the radiating face of the transducer is immersed in a fluid taken in a semi-rigid container, we have to take into account the effect of reflections. It is observed that, there exist a certain phase lag β between the driving signal and the radiating signal, so that the reflected signal can be represented as,

$$F'(t) = k'F \sin (\omega t - \beta + \beta') \qquad (V.2)$$

where the quantity k' depends on the impedance at resonance, the efficiency of radiation, the directivity pattern and the reflectivity of the bottom surface of the container and

$$\beta' = \frac{2\pi}{\lambda} 2h$$

$$= \pi, \text{ if } h = \lambda/4$$

$$= 2\pi, \text{ if } h = \lambda/2$$

h being the height of the castor oil column below the radiating face of the transducer.

Here the analysis is limited to the following two specific cases of the reflected signal, depending on the position of the transducer.

(i) Reflected signal opposes the vibration and

(ii) Reflected signal enforces the vibration.

Case (i): Reflected signal opposes the vibration

In this case, the differential equation (V.1) takes the form,

$$M_1 \frac{du_1}{dt} + R_{m1} u_1 + \frac{1}{C_{m1}} \int u_1 dt = F \sin \omega t - k'F \sin (\omega t - \beta_1)$$

$$= F \sin \omega t - k'F \sin \omega t \cos \beta_1 + k'F \cos \omega t \sin \beta_1$$

$$= F \sin \omega t(1 - k' \cos \beta_1) + k'F \cos \omega t \sin \beta_1$$

$$= a'F \sin \omega t \cos \theta_1 + a'F \cos \omega t \sin \theta_1$$

$$\text{i.e.,} \quad M_1 \frac{du_1}{dt} + R_{m1}u_1 + \frac{1}{C_{m1}}\int u_1 dt = a'F \sin(\omega t + \theta_1) \quad \ldots (V.3)$$

where

$$\tan \theta_1 = \frac{k' \sin \beta_1}{1 - k' \cos \beta_1} \quad \text{and} \qquad (V.4)$$

$$a' = \sqrt{(1 + k'^2 - 2k' \cos \beta_1)} \qquad (V.5)$$

Case (ii): Reflected signal enforces the vibration

Here, equation (V.1) has the form,

$$M_2 \frac{du_2}{dt} + R_{m2} u_2 + \frac{1}{C_{m2}}\int u_2 \, dt = F \sin \omega t + k'F \sin (\omega t - \beta_2)$$

$$= F \sin \omega t + k'F \sin \omega t \cos \beta_2 - k'F \cos \omega t \sin \beta_2$$

$$= F \sin \omega t (1 + k' \cos \beta_2) - k'F \cos \omega t \sin \beta_2$$

$$= b'F \sin \omega t \cos \theta_2 - b'F \cos \omega t \sin \theta_2$$

$$\text{i.e.,} \quad M_2 \frac{du_2}{dt} + R_{m2}u_2 + \frac{1}{C_{m2}}\int u_2 dt = b'F \sin (\omega t - \theta_2) \quad \ldots (V.6)$$

where

$$\tan \theta_2 = \frac{k' \sin \beta_2}{1 + k' \cos \beta_2} \qquad (V.7)$$

and

$$b' = \sqrt{(1 + k'^2 + 2k' \cos \beta_2)} \qquad (V.8)$$

The solution of equation (V.1) can be written in the form,

$$u = \frac{v}{\frac{R_m}{\alpha} + \frac{j}{\alpha}\left(\omega M - \frac{1}{\omega C_m}\right)} \qquad (V.9)$$

where v is the voltage applied across the element. In an analogous manner, equations (V.3) and (V.6) can be solved and these solutions yield,

$$\begin{aligned} M_1 &= \frac{M}{a'} \\ R_{m1} &= \frac{R_m}{a'} \\ C_{m1} &= a' C_m \end{aligned} \qquad (V.10)$$

$$\begin{aligned} M_2 &= \frac{M}{b'} \\ R_{m2} &= \frac{R_m}{b'} \\ C_{m2} &= b' C_m \end{aligned} \qquad (V.11)$$

These relations predict variations of M, R_m and C_m with depth of immersion.

Hence, it can be concluded that, the observed variation of impedance at resonance is the direct result

of the variations in M, C_m and R_m. Hence, by adjusting the depth of immersion, it is possible to match the resistive component of the impedance of the transducer at resonance, to that of the generator. The reactive component will be tuned out using an inductance coil.

The electrical equivalent circuits of the transducer without and with the container in the two specific cases are shown in Fig. A.V.1.

Evaluation of k

The average acoustic power radiated by the transducer element driven by the force F sin ωt is given by [43],

$$P = \frac{1}{2} R_m u^2 \qquad (V.12)$$

The current flowing through the circuit, associated with the element is related to the velocity amplitude by [1]

$$i = \alpha u \qquad (V.13)$$

The driving force F is given by

$$F = \alpha v \qquad (V.14)$$

Combining equations (V.13) and (V.14),

$$F = \frac{i}{u} v$$

$$= \frac{P_e}{u} \qquad (V.15)$$

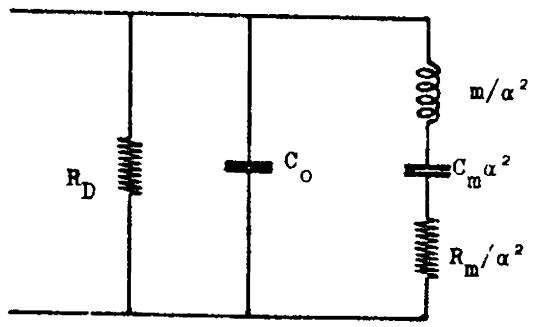

Fig.A.V.1(i)

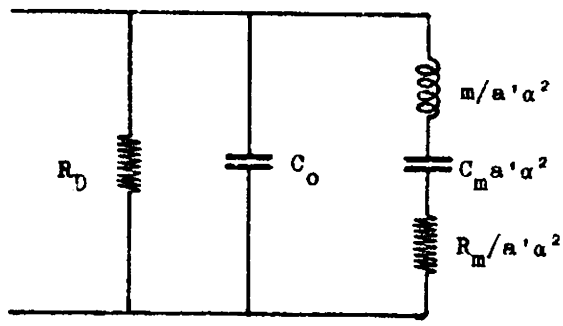

Fig.A.V.1(ii)

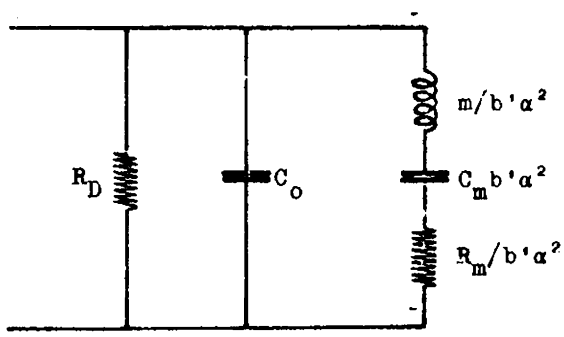

Fig.A.V.1(iii)

Fig.A.V.1(i) : Electrical elements of the transducer without the container

Fig.A.V.1(ii): Electrical elements of the transducer with the container, corresponding to the case when the reflected wave opposes the vibration

Fig.A.V.1(iii): Electrical elements of the transducer with the container, corresponding to the case when the reflected wave enforces the vibration

where

P_e = the peak electrical power pumped to the element.

The efficiency of radiation

$$\eta = \frac{P}{P_e}$$

$$\text{or } P = P_e \eta$$

$$= \eta F u \qquad \text{(V.16)}$$

Here P is the acoustic power radiated to the infinite medium. When the transducer is immersed in a finite medium, the signal reflected from the bottom of the container will alter its performance as is clear from the results presented in chapter VI. When the reflected signal opposes the vibration, the driving force becomes,

$$F_1(t) = a'F \sin \omega t$$

In this case, the radiated acoustic power is

$$P_1 = \eta_1 F u_1 a' \qquad \text{(V.17)}$$

Similarly, when the reflected signal enforces the vibration, the acoustic power takes the form

$$P_2 = \eta_2 F u_2 b' \qquad \text{(V.18)}$$

$$\therefore \quad \frac{P_1}{P} = a' \frac{u_1}{u} \frac{\eta_1}{\eta}$$

$$\text{or} \quad \frac{P_1}{P} = a' \frac{i_1}{i} \frac{\eta_1}{\eta} \qquad (V.19)$$

$$\text{or} \quad \frac{p_1^2}{p^2} = a' \frac{i_1}{i} \frac{\eta_1}{\eta} \qquad (V.20)$$

where

i = current in the circuit when the transducer is radiating into infinite medium.

i_1 = current in the circuit when the transducer is radiating into the finite medium.

p = peak acoustic pressure in the infinite medium.

p_1 = peak acoustic pressure in the finite medium.

Thus, knowing the values of p, p_1, i, i_1, η, η_1 and β_1, k' can be evaluated using equations (V.5) and (V.20).

The variation of the radiated acoustic pressure level, measured at a distance of 1m from the projector, with depth of immersion can be explained using the results of this analysis. When the reflected signal opposes the vibration, the acoustic power radiated will

be less, in agreement with (V.17) while the enforcing case yields more acoustic power as per (V.18).

The theoretical analysis presented in this appendix clearly explains the cause for the variation of M, C_m, R_m and the efficiency of radiation.

R E F E R E N C E S

R E F E R E N C E S

[1a] Tucker, D.G., and Gazey, B.K.: 'Applied Underwater Acoustics', Pergamon Press London (1966), pp. 2 - 18

[1b] Ibid. pp. 135 - 144

[1c] Ibid. pp. 150 - 160

[2] Bell, T.G.: 'Sonar and Submarine Detection', U.S. Navy Underwater Sound Lab. Rep. 545 (1962)

[3a] Robert J. Urick : 'Principles of Underwater Sound', McGraw-Hill Book Company (1975), pp. 1 - 12

[3b] Ibid. pp. 56 - 60

[3c] Ibid. pp. 70 - 78

[4a] 'Transducer Technology - Proceedings of the Symposium held in May 1975': Naval Physical and Oceanographic Laboratory, Cochin. (Printed at the INSDOC Regional Centre, Bangalore, India) pp. 81 - 84

[4b] Ibid. pp. 107 - 111

[4c] Ibid. pp. 112 - 115

[5] Ward Widener, M.: 'The Development of High-efficiency Narrow-band Transducers and Arrays', J. Acoust. Soc. Am., 67: 1051 (1980)

[6] Davids, N., Thurston, E.C., and Heuser, R.E.: 'The Design of Optimum Directional Acoustic Arrays', J. Acoust. Soc. Am., 24: 50 (1952)

[7] Albers, V.O.: 'Underwater Acoustics Handbook', Pennsylvania State University Press, University Park, Pa. (1960) Chap. 11

[8] Dolph, C.L.: 'A Current Distribution for Broad-side Arrays which Optimises the Relationship Between Beamwidth and Side Lobe Level', Proc. IRE, 34 : 335 (1946)

[9] '50 Years of Ocean Engineering': Catalogue of Edo Western Corporation, Salt Lake City, Utah.

[10] 'Acoustic Transducers' : Catalogue of Edo Western Corporation, Salt Lake City, Utah.

[11] Carson, D.L.: 'Diagnosis and Cure of Erratic Velocity Distributions in Sonar Projector Arrays', J. Acoust. Soc. Am., 34: 1191 (1962)

[12] Karnovskii, M.L.: 'Calculations of the Radiation Resistance of Several Types of Distributed Systems', Sov. Phys. Acoust., 2 : 200 (1956)

[13] Rusby, J.S.M.: 'Investigations of a Mutual Radiation Impedance Anomaly between Sound Projectors Mounted in an Array', Acustica, 14: 127 (1964)

[14] Eicher, E. : 'Calculation of Coupling Effects in Prichard's Array', J. Acoust. Soc. Am., 36: 1393 (1964)

[15] Arase, E.M.: 'Mutual Radiation Impedance of Square and Rectangular Pistons in a Rigid Infinite Baffle', J. Acoust. Soc. Am., 36: 1521 (1964)

[16] Stumpf, F.B., and Lukman, F.J.: 'Radiation Resistance of Magnetostrictive - Stack Transducer in Presence of Second Transducer at Air-Water Surface', J. Acoust. Soc. Am., 32: 1420 (1960)

[17] Waterhouse, R.V.: 'Radiation Impedance of a Source Near Reflectors', J. Acoust. Soc. Am., 35: 1144(1963)

[18] Sherman, C.H.: 'Theoretical Model for Mutual Radiation Resistance of Small Transducers at an Air-Water Surface', J. Acoust. Soc. Am., 37: 532(1965)

[19] Waterhouse, R.V.: 'Mutual Impedance of Acoustic Sources', Paper J21, 5th International Congress on Acoustics, September 1965.

[20] Berktay, H.O.: 'Possible Exploitation of Nonlinear Acoustics in Underwater Transmitting Applications', J. Sound Vib. 2(4) : 438 (1965).

[21] Dun, D.J., Kuljis, M., and Welsby, V.G.: 'Nonlinear Effects in a Focussed Underwater Standing-wave Acoustic System', J. Sound Vib. 2(4), 471 (1965)

[22] Francis Hugh Fenlon: 'On the Maximum Achievable Conversion Efficiency of a Parametric Acoustic Array', Proc. ICASSP '78, pp. 127 - 129

[23] Tucker, D.G.: 'Sonar in Fisheries - A Forward Look', Trustees, The Buckland Foundation (1967), pp. 113-125

[24] Berktay, H.O.: 'Some Proposals for Underwater Transmitting Applications of Nonlinear Acoustics', J. Sound Vib. 6(2): 244 (1967)

[25] Truchard, J.J. : 'Parametric Receiving Array and the Scattering of Sound by Sound', J. Acoust. Soc. Am., 64 : 280 (1978)

[26] Truchard, J.J.: 'Parametric Acoustic Receiving Array I - Theory', J. Acoust. Soc. Am., 58: 1141 (1975)

[27] Berktay, H.O., and Al-Temimi, C.A.: 'Scattering of Sound by Sound', J. Acoust. Soc. Am., 50: 181 (1969)

[28] Bellin, J.L.S., and Beyer, R.T.: 'Experimental Investigations of an End-Fire Array', J. Accust. Soc. Am., 34: 1051 (1962)

[29] Uno Ingard and David C. Pridmore Brown: 'Scattering of Sound by Sound', J. Acoust. Soc. Am., 28: 367 (1956)

[30] Wallace Dean III, L. : 'Interaction Between Sound Waves', J. Acoust. Soc. Am., 34: 1039 (1962)

[31] Joie Pierce Jones, Robert T. Beyer: 'Scattering of Sound by Sound', J. Acoust. Soc. Am., 48: 398 (1970)

[32] Tucker, D.G.: 'The Exploitation of Nonlinearity in Underwater Acoustics', J. Sound Vib. 2(4): 429 (1965)

[33] Barnard, G.R., Willette, J.G., Truchard, J.J., and Shooter, J.A.: 'Parametric Acoustic Receiving Array', J. Acoust. Soc. Am., 52 (5) (1972)

[34] Berktay, H.O.: 'Parametric Amplification by the use of Acoustic Nonlinearities and some possible Applications', J. Sound Vib. 2(4): 462 (1965)

[35] Westervelt, P.J.: 'Parametric Acoustic Array', J. Acoust. Soc. Am., 35: 535 (1963)

[36] 'Design and Construction of Magnetostriction Transducers', Summary Technical Report of Division 6, NDRC, Vol.13, p.279

[37] Preferred Reference Quantities for Acoustical Levels, ANSI S 1.8 - 1969, American National Standards Institute, New York.

[38] Donald G. Fink, and Alexander A. Mckenzie: 'Electronics Engineers' Handbook', McGraw-Hill Book Company (1975), 25 - 124

[39] Bernard D. Steinberg: 'Principles of Aperture and Array System Design', John Wiley and Sons, Inc.(1976), Chap. 14

[40] Stephens, R.W.B.: 'Underwater Acoustics', John Wiley and Sons Ltd. (1970), p. 208

[41] Saseendran Pillai, P.R., and Sridhar, C.S.:'Tuning of Transducer Elements in a Transducer Array', Electron. Lett., 16: 606 (1980)

[42] Saseendran Pillai, P.R., and Sridhar, C.S.: 'Side Lobe Suppression in a Directional Transducer Array - Design Considerations', Accepted for publication in 'Acoustics Letters' and will appear in Vol.5, No.1 (August 1981) issue.

[43] Charles H. Sherman: 'Effect of the Near-field on the Cavitation Limit of Transducers', J. Acoust. Soc. Am., 35: 1409 (1963).